CHAPTER

3

Time-Domain Models

P. Ricci

Orwell Offshore, London, United Kingdom

(Formerly at Global Maritime Consultancy Ltd., Tecnalia Research and Innovation and Instituto Superior Técnico, Lisbon)

3.1 INTRODUCTION AND FUNDAMENTAL PRINCIPLES

The frequency-domain numerical techniques presented in Chapter 2 are fundamental for the full comprehension of the dynamics of wave energy converters (WECs) and their underlying working principles, but depend on the system being linear. However, the power take-off (PTO) configurations applied on the majority of the WECs under development involve very complex systems that can be modelled satisfactorily only by introducing nonlinearities in the mathematical model of the energy extraction mechanism. Most of the control strategies proposed for wave power extraction are also highly nonlinear (Hoskin and Nichols, 1987; Babarit and Clément, 2006; Babarit et al., 2009) and additional elements in the model, such as moorings or structural components, may also be nonlinear. To prove the validity of a PTO design or a control strategy, a model that is more realistic than a frequency-domain model is often needed, particularly when real sea-state performance is the determining criterion to validate a solution. In such cases, a time-domain model is generally unavoidable.

Time-domain models are capable of dealing with the nonlinearities arising from the different elements of the energy chain as well as more complex formulations for fluid interaction and damping mechanisms that result in nonlinear hydrodynamic forces. Furthermore, they allow modelling transient situations that are impossible to characterize in a frequency-domain approach, which are applicable solely to stationary processes. Such transient cases are often critical in practice (e.g. the failure of a component) or might be associated with the effective working principle of a device (e.g. a valve shutting in extreme waves, a brake activated when the motion amplitudes exceed a defined threshold). On the other hand, time-domain methods are significantly more computationally exigent than frequency-domain approaches. Because of this they are typically employed at the later stages of the design process, when many features of the WEC are already established and the focus of the development has moved to the design of the PTO and the definition of the control strategy.

In a general sense, time domain here refers to the possibility of deterministically computing the dynamics of floating bodies directly in time, with no reference to the properties of the process (e.g. harmonic, stationary, ergodic). As such, many different methods might be classified as 'time-domain methods' and some of them might involve alternative formulations of the hydrodynamic

http://dx.doi.org/10.1016/B978-0-12-803210-7.00003-7

wave-body interaction problem with a representation of the hydrodynamic loads different from the typical terminology adopted from diffraction–radiation analysis. However, this chapter only considers time-domain models that are based specifically on the Cummins equation (1962). This approach has been applied extensively and has proven effective in a large number of applications; other approaches that could also be considered to be time-domain models are covered in Chapters 5 and 6. Furthermore, its foundations lie in the same principles that constitute the basis of the frequency-domain approach and thus its results can be linked directly with those derived from frequency-domain models from early development stages.

This chapter begins by reviewing the general formulation of the Cummins method with reference to the case of wave energy conversion. The methodology to represent the wave excitation forces is presented with an insight on the randomness of the simulated wave signal and its consequence on the statistical properties of the results. The requirement for a convolution integral to be included in the equations of motion to account for radiation forces gives rise to a variety of numerical methods and approaches which will be briefly presented and reviewed. The consequences of different choices on the numerical approach for time-domain analysis are illustrated by making reference to a simple type of WEC: a cylindrical point-absorber connected to either a linear or a hydraulic PTO. Particular attention is given to the estimation of power extracted with a discussion on the effect of the duration of the simulation on its assessment. Finally, the power and the limitations of the presented tools are discussed with a mention of the existing challenges still being tackled by the wave energy community.

3.2 THE CUMMINS EQUATION FOR MODELLING WECs

Because the majority of WECs can be represented as a system of floating bodies, their dynamics can be described, at least from the most basic principles, by mathematical models that have been extensively developed for the offshore and ship industry. The assumption that the hydrodynamics can be considered to be linear leads to the application of the time-domain formulation first proposed by Cummins (1962), which is based on a system of integro-differential equations.

Applying the Cummins equation for a generic floating body subject to the action of wave forces F^{wav} and other external forces F^{ext}, and assuming an inertial system of reference centred on its initial position, the motion x_j in the 'j' direction can be described by the expression:

$$\sum_{j=1}^{6}\left(\left(M_{ij}+A_{ij}^{\infty}\right)\ddot{x}_j(t)+\int_{-\infty}^{t}K_{ij}(t-\tau)\dot{x}_j(\tau)d\tau+C_{ij}\left(x_j\right)\right)=F_i^{\mathrm{wav}}(t)-F_i^{\mathrm{ext}}(x,\dot{x},t) \tag{3.1}$$

where M_{ij} and C_{ij} represent elements of the mass and restoring coefficient matrix respectively and A_{ij}^{∞} is the added mass at infinite frequency, given by:

$$A_{ij}{}^{\infty}=\lim_{\omega\to\infty}A_{ij}(\omega) \tag{3.2}$$

where $A_{ij}(\omega)$ is the frequency-dependent added mass introduced in the Chapter 2. $K(t)$ is the radiation impulse response function (RIRF) or memory function (so called because it represents a memory effect due to the past motion of the body).

Although the hypothesis of linearity in the fluid-structure interaction might appear to limit its application, the formulation is very powerful because all the nonlinearities arising from other components, such as the PTO and moorings, can be included in the term F^{ext}.

We should note that the convolution integral in Eq. (3.1) is evaluated from minus infinity to the present time instant. This is equivalent to stating that the time history of the response is solely dependent on the past values of the forcing function. In other words, according to this formulation, the system is causal. The causality

of the response of a floating body with respect to the action of external forces and moments has been discussed thoroughly in the past and has been demonstrated by Wehausen (1992) as a consequence of the radiation condition of water waves. However, when considering the wave elevation at a specified monitoring point as input to the system, the related IRF can no longer be considered causal (Falnes, 1995) and this has important consequences on the design of control systems for WECs as will be briefly commented in Section 3.3.3.

We should also note that the formulation given in Eq.(3.1) is valid only for stationary floating bodies, ie, bodies that are not advancing in the water. As shown by Ogilvie (1964), the assumption of a finite forward speed modifies slightly the formulation of the Cummins equation by requiring additional linear damping terms and a different derivation for the RIRF. However, we will assume that all the WECs are effectively stationary so we are not concerned with the additional complication that nonstationary bodies bring.

The Cummins equation can effectively be defined using a set of ordinary differential equations (ODEs), which can be solved numerically by using one of the many numerical methods available (Conte and De Boor, 1980; Riley et al., 2006). There is no limit to the number of degrees of freedom that can be modelled with the Cummins approach. Because of the linearity assumption, the fluid forces due to the motion in any degree of freedom can be treated separately with a specific convolution and added mass term. This means that both simple and complex WECs, with different constraints and connections, can be modelled by a system of ODEs using the same fundamental approach.

The formulation of a set of ODEs that represent a WEC requires consideration of four distinct aspects, which are detailed in the subsequent sections. The first section (Section 3.3) deals with the definition of the wave excitation force, the second section (Section 3.4) deals with the generation of the RIRF, the third section (Section 3.5) deals with the solution of the convolution integral and the final section (Section 3.6) deals with the hydrostatic force.

3.3 WAVE EXCITATION FORCES

3.3.1 Wave Loads in Time-Domain Models

In wave energy conversion models, the energy carried by propagating ocean waves is introduced into the system by the action of the so-called wave 'excitation' forces. Indeed, the term 'excitation' makes direct reference to the classical image of a damped oscillator being excited by external forces. It is customary (Faltinsen, 1993; Chakrabarti, 2005) to split the contributory wave forces on moored floating structures into three components:

- Steady mean drift force
- First-order excitation forces (typically oscillating with the frequency of the incident waves)
- Slow-drift forces (predominantly oscillating with lower frequencies than the ones of the wave spectrum)

Potentially, other contributions might arise (e.g. high-frequency drift forces for very stiff systems like tension leg platforms) but these components as previously given are sufficient to properly simulate the response of floating structures in the vast majority of cases.

All of these forces can be obtained from a potential flow model, introduced in the previous chapter, and can be determined by the same packages used for the computation of hydrodynamic coefficients (ANSYS AQWA, 2010; WAMIT, 2004). However, their importance in system dynamics is different depending on the type of system and the objective of the analysis. In the vast majority of cases only the first-order excitation forces are significant and included in the model.

Drift forces can be very important for the design and analysis of mooring systems but are typically neglected in a preliminary approach when analyzing the first-order motion of a device. Indeed, for slack-moored devices, the influence of the drift forces on the wave-frequency oscillating dynamics of the device is minimal to the point that a common procedure applied for mooring design in offshore engineering is to separate the first-order dynamics of the platform from those of the moorings.

Furthermore, because these forces are proportional to the square of the wave amplitude, they are expected to be most significant for very large waves, possibly far from the typical operational conditions for wave energy absorption. If, however, the scope of the analysis required their application (e.g. when performing simulations to design the moorings) their introduction into the time-domain system would not represent a major issue, provided that appropriate quadratic transfer functions were determined from hydrodynamic analysis (Pinkster, 1980).

3.3.2 Excitation Forces as Superposition of Harmonic Components

As stated previously, for the purpose of modelling a WEC, the sole consideration of the first-order excitation forces is generally sufficient to provide a reliable estimate. In regular monochromatic waves, we can express the excitation force acting on the 'j' mode as

$$F_{ej}(t) = \Gamma(\omega) A \cos\left(\omega t + \phi(\omega)\right) \tag{3.3}$$

where we have introduced an excitation force coefficient $\Gamma(\omega)$ and a phase angle $\phi(\omega)$, both frequency dependent and that can be obtained directly from the boundary integral equation method described in the previous chapter (see Section 2.4.1). We note that the excitation force is directly proportional to the wave amplitude A.

The phase angle represents the difference in time between a peak in the incident wave profile at the reference point and a peak of the excitation force. The reference point is normally chosen to be the centre or other notable point of the WEC; however, the selection of the reference point also has some relevant implications in the causality of the excitation force signal, which will be discussed later. Eq. (3.3) considers positive phase angles as 'leads' and negative phase angles as 'lags'. In other words, if the phase is positive, the excitation force leads the incident wave by a certain fraction of the period.

When considering systems of one degree of freedom and in absence of sophisticated control systems acting on the basis of the sea-surface elevation, the information on the phase angle of the excitation force does not affect the dynamics of the body and can be neglected. However, the information on the phase angle is very important in systems with multiple degrees of freedom because of the difference in phases between the excitation forces acting on different degrees of freedom.

Since, as assumed in Eq. (3.3), the excitation force generated by an incident wave is a harmonic function with a module directly proportional to the wave amplitude, the most straightforward procedure to model first-order wave forces in irregular waves is the simple linear superposition of N independent sinusoidal components (ideally, $N \to +\infty$) such as

$$F_{ej}(t) = \sum_{i=1}^{N} \Gamma(\omega_i) A_i \cos\left(\omega_i t + \phi(\omega_i) + \varphi_i\right) \tag{3.4}$$

The amplitudes A_i of each frequency component are defined from the energy spectral density $S(\omega)$ as *Rayleigh* distributed random values with a mean square value of $2S(\omega_i)\Delta\omega_i$. The wave surface elevation phases φ_i are randomly selected assuming a uniform distribution within $[0;2\pi]$. With this assumption, the randomness of the elevation process is properly reproduced and its statistical properties are correctly modelled. An alternative method that is commonly used is based on using directly the deterministic value $\sqrt{2S(\omega_i)\Delta\omega_i}$ for the amplitudes.

The main undesirable consequences of not selecting the amplitudes randomly lie in the statistical properties of the elevation process (in particular wave groupiness) which may not agree with theory and even distort those related to the mean performance of WECs drawn from numerical simulations. Each sea-surface elevation signal should be simulated taking this important theoretical aspect of wave modelling into account (see Fig. 3.1).

However, as shown by Saulnier et al. (2009), the mean extracted power estimation does not seem to be appreciably influenced by the inherent inconsistency of the deterministic method, widely implemented in many offshore numerical applications. This suggests that this method can be used to estimate the mean power extracted in a given target sea-state provided the size of the realizations is significant in terms of simulating duration, number of samples or number of simulated waves.

The error on the mean power estimation is always reduced when using the deterministic method instead of the more correct random one for simulating the input wave signal, whatever the model. Moreover, this reduction is amplified with simulation duration T_d. It is therefore advantageous for developers to use the standard method with deterministic amplitudes when the length and number of simulations has to be limited. Let us emphasize though that, as shown in Section 3.9, the estimator's standard deviation in nonlinear simulations seems to follow a $1/T_d^{-1/2}$ law still when using the more correct method with randomly distributed amplitudes, so that the power estimation error against T_d may be predicted by choosing this method.

To be numerically computable, the summation in Eq. (3.4) has to be taken over a discrete number of frequency components. The choice of the number of frequency components N required to model the excitation force needs to be carried out cautiously to avoid unrealistic results. The most straightforward way of choosing the frequencies for the modelling of the excitation forces consists in applying an arithmetic progression where $\omega_i = i\Delta\omega$ where $\Delta\omega$ is the fundamental frequency step (the minimum frequency). Clearly, this approach would generate a periodical time series that would repeat exactly

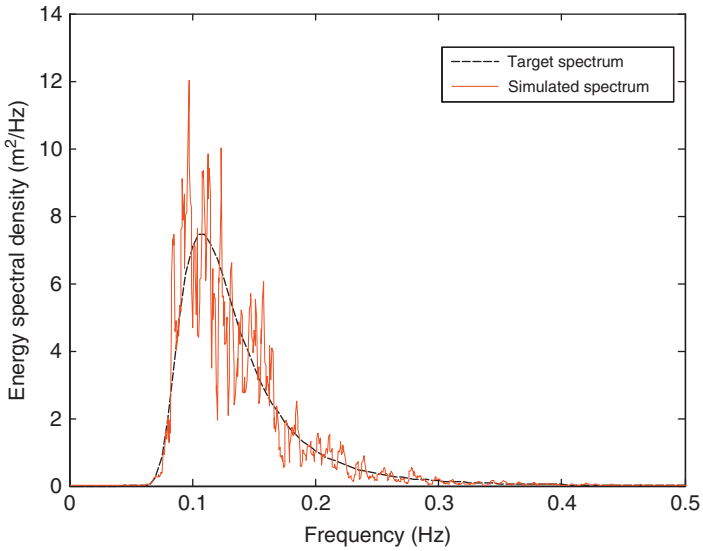

FIG. 3.1 Target Bretschneider and (smoothed) simulated spectrum.

after $2\pi/\Delta\omega$ and to avoid repeatability, one should either limit the duration of the simulation to less than that or pick a smaller frequency step. A smaller frequency step with an arithmetic progression invariably results in a large number of frequency components and consequently a longer time to compute the incident wave force time series.

A simple method to avoid repeatability is the application of a geometric progression to the sequence of frequencies so that each frequency is defined as

$$\omega_i = a\omega_{i-1} = a^{i-1}\omega_1 \tag{3.5}$$

where a is a properly chosen constant that relates successive values of the frequency sequence. If a maximum frequency $\omega_{\max}$ is defined, then $a = (\omega_{\max}/\omega_1)^{N-1}$ where N is the number of components.

Both the arithmetic and geometric progressions might not be suited to model peculiar spectral shapes with a large amount of energy concentrated in a very small frequency range. A further alternative to these approaches is offered by the so-called equal energy method, where the frequencies are selected in such a way that the energy contained in each frequency interval is the same. This leads to finer discretization close to the peak frequencies which generally allows reproducing the signal with fewer components than the ones used for the arithmetic progression. Moreover, since the frequencies are not evenly distributed, this method is less prone to repeatability.

An example of the discretization of a Bretschneider wave spectrum with $H_s = 3$ m and $T_e = 8$ s into 10 wave components using the three methods outlined above is presented in Fig. 3.2.

The number of components used here, 10, has been selected to highlight the difference between the methods and is much smaller than normally recommended. Standard practice suggests that at least 300 components are required to produce accurate results for simulations longer than 30 min. If the arithmetic progression approach is used, the number of components is automatically established by the duration of the simulations and the selected maximum frequency (eg, 1200 wave components are required for a simulation lasting 1800 s and maximum frequency of 0.6 Hz).

It is important to understand, however, that, regardless of the discretization method, the final

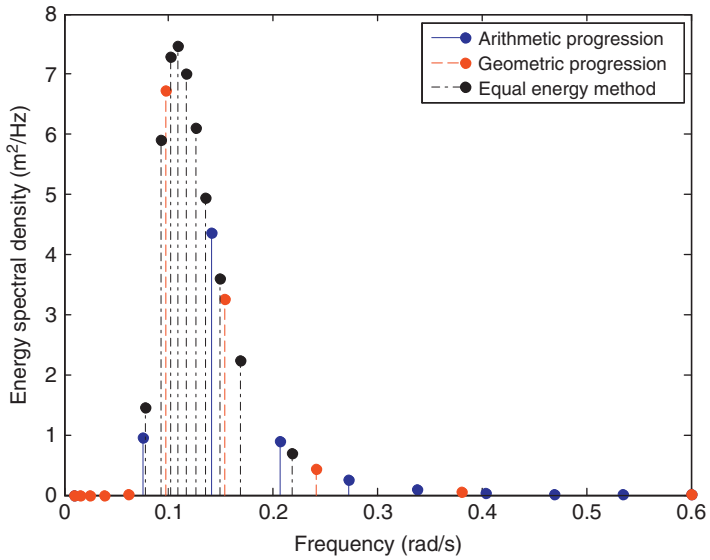

FIG. 3.2 Discretization of wave spectrum into 10 frequency components using different methods.

result would always be a sum of harmonics and therefore some repetition is expected after a certain time. For this reason, the choice of the frequency range should always be directly related to the required duration of the simulation.

3.3.3 Convolution of the Excitation Force

The excitation force in the time domain is formally related to its frequency-domain expression by an inverse Fourier transform (Falnes, 2002). Indeed, the formulation given by Eq. (3.4) can be interpreted as a discrete representation of the inverse Fourier transform of the excitation force in the frequency domain where, by selecting a certain set of frequency and phases, we had implicitly assumed the knowledge of the wave elevation time history.

However, if the input surface elevation is taken as the signal recorded at a certain point of reference O on the free surface with coordinates $x=x_0$ and $y=y_0$, then the correct representation of the wave excitation force in the 'j' degree of freedom is formally given by

$$F_{ej}(t)=\int_{-\infty}^{+\infty} h_{fj}(\tau)\eta(x_0,y_0,t-\tau)\,d\tau \tag{3.6}$$

where $h_{fj}(t)$ is the impulse response function (IRF) of the wave excitation force and $\eta(x_0,y_0,t)$ is the wave elevation measured at O at the time t.

The convolution integral in Eq. (3.6) is taken over the whole time history (from minus infinity to plus infinity). This means that, in theory, knowledge of the surface elevation in the future is required to provide an estimate for the excitation force, unless it can be proven that the IRF is causal, ie, it is equal to zero for $t<0$. However, as shown by Falnes (1995), the IRF of the wave excitation force acting on a floating body is, in general, not causal. The concept of noncausality can be easily understood when the wave elevation is defined with respect to a point placed in the vicinity of the floating body, such as the centre of the water-plane area. In this case, the body will experience a force before the wave crest has effectively reached the centre of its water-plane area (King and Beck, 1987; Korsmeyer, 1991). Moreover, even if the reference point is chosen outside the body and on the 'upstream' side, this does not guarantee that the associated IRF is causal. In fact, it has been shown (Falnes, 1995) that, for a heaving cylinder, a spatial shift of the order of 6 radii would be required to generate an IRF that is approximately causal.

The effect of a change in the point of reference can be easily analysed. Considering two points of reference O and P separated by a distance L in the direction of the wave propagation, the transfer functions of the excitation force with respect to the wave elevation measured at the two points are related by the expression:

$$H_{fj\mathrm{P}}(\omega)=H_{fj\mathrm{O}}(\omega)\mathrm{e}^{\mathrm{i}k(\omega)L} \tag{3.7}$$

where the point P is assumed located downstream of the point O. The wavenumber $k(\omega)$ is found by the dispersion relationship. An example for a floating cylinder of radius and draught equal to 5 m is shown in Fig. 3.3, where the IRFs corresponding to the choice of three different points of reference are plotted.

As seen from Fig. 3.3, if the point of reference is taken approximately 6 radii upstream from the centre of the cylinder (defined here at $x=0$), the IRF is almost causal, although it is still finite for $t<0$ over a relatively small interval.

Since time-domain models are purely numerical, it is possible to know the wave excitation force in advance. Thus, we are not concerned with the practical difficulties of predicting the excitation force (or the wave elevation) at a specified position. In real systems deployed at sea this is not possible since any estimation of the excitation force would be based on wave elevation measurements and the IRF related to the wave measurements is generally not causal. The problem of short-term wave forecasting and its implementation in real-time control of WECs has been treated by a number of authors (Tedd and Frigaard, 2007; Fusco and Ringwood, 2012) and it might be important when considering control strategies.

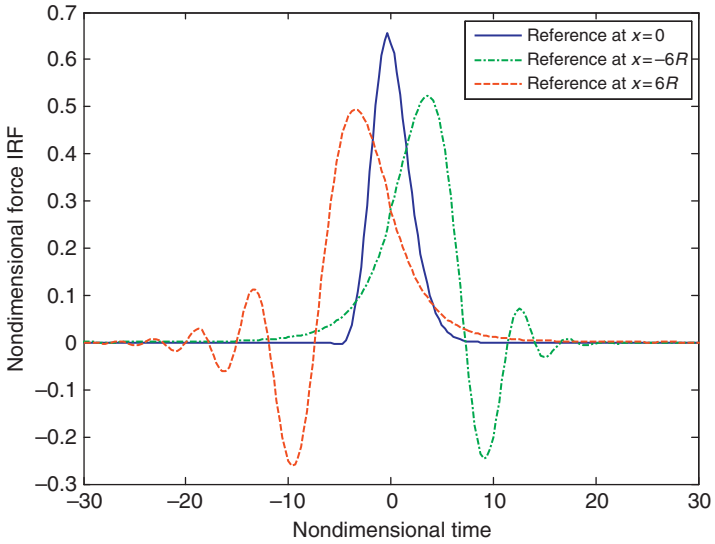

FIG. 3.3 Impulse response function of the wave excitation force on a heaving cylinder with radius/draught ratio equal to 1 and radius equal to R floating in infinite water depth, for different points of reference for the definition of the impulse wave ($x=0$ corresponds to the centre of the cylinder). Time and IRF are nondimensionalized by factors $\sqrt{(R/g)}$ and $\rho\sqrt{g^3R^3}$ respectively.

The use of the formulation given by Eq. (3.4) allows avoiding the computation of the convolution integral given by Eq. (3.6). This is the general procedure applied by most modellers although its benefit in terms of computational time is not always apparent since it depends largely on the number of frequency components applied. On the other hand, the convolution integral can be useful when the modeller wants to apply a state-space approach for the modelling of the excitation force, as seen, for example in Yu and Falnes (1996) and in McCabe et al. (2005). This state-space approach will be presented for the RIRF integral in Section 3.5. Its application to the excitation force is very similar with the important caveat that the excitation force IRF needs to be casualized before being converted into a state-space model.

3.3.4 Nonlinear Wave Forces

Although the solution of the potential flow model is fundamentally linear, it is possible to abuse the solution to include what is typically referred to as a nonlinear Froude–Krylov force (Gilloteaux et al., 2007). The Froude–Krylov force is the force on the body calculated by integrating over the wetted surface the incident wave pressure (see Section 2.4.1.1.1). In the standard linear calculation of the Froude–Krylov force the mean position of the body and water-plane is used to determine the surface integral in accordance with the assumption of the linear potential flow theory (see Section 2.3). In the nonlinear Froude–Krylov force the instantaneous positions of the body and water-plane are used.

Inclusion of the nonlinear Froude–Krylov force within the incident wave force becomes especially important when the wetted surface changes significantly either due to the amplitude of the incident wave, the amplitude of the body motions or a combination of the two. It is clear that this will be the case for small bodies in large waves, but it may also be relevant where the body is flared close to the water-plane. It is also worth noting that inclusion of the nonlinear Froude–Krylov force is most useful where

the incident wave force is dominated by the Froude–Krylov force. This is the case for the heave force on small bodies, but is less true for surge/pitch forces, or for larger bodies.

A further abuse of linear wave theory can be achieved by the additional calculation of diffraction force using the instantaneous position of the body (McCabe et al., 2006). It should be clear that these types of representation are not mathematically correct; however, they have consistently been found to result in an improvement of a model's accuracy when included (provided that these nonlinear forces are significant).

Calculation of the nonlinear Froude–Krylov force is relatively straightforward since it simply requires knowledge of the instantaneous positions of the body and water surface. However, the calculation of the nonlinear diffraction force is more complex because it involves modification of the IRF for the convolution integral for the wave force given in Eq. (3.6). McCabe et al. (2006) provide an ingenious solution to this problem by representing the convolution integral using a set of state-space parameters that are a function of the body position. The instantaneous wave force is then calculated by parameter interpolation. The reader is referred to the paper by McCabe et al. (2006) for more details.

3.4 THE RIRF

3.4.1 Properties of the RIRF

The computation of the convolution integral in Eq. (3.1) involves the determination of the RIRF defined as the IRF corresponding to a velocity impulse. This convolution is associated with a memory effect caused by the presence of the free surface. Indeed, past motions of the body generate waves which keep on propagating long after the motions have stopped. The forces acting on the body as the result of these radiated waves are modelled by the convolution of the RIRF with the body velocity. As this direct relation with wave radiation suggests, the RIRF can be derived from the hydrodynamic coefficients introduced in Chapter 2 to model the wave radiation in the frequency domain.

We know that the radiation damping coefficient and the added mass are related to the real and imaginary part of the radiation force due to unitary oscillation amplitude. If we consider the velocity amplitude as an input to the dynamic system, then this unitary radiation force can be assumed to be a frequency-domain transfer function for the radiation force so that we can write, for the force acting on the degree of freedom '*i*' due to a motion in the degree of freedom '*j*':

$$\hat{F}_{ij}(\omega) = \hat{U}_j \hat{f}_{ij}(\omega) \tag{3.8}$$

where $\hat{F}_{ij}$ is the Fourier transform of the radiation force, $\hat{U}_j$ is the velocity in the '*j*' degree of freedom and $\hat{f}_{ij}$ is the radiation transfer function (RTF). According to the definition of added mass and damping coefficient, we have

$$\omega A_{ij} = \mathrm{Im}\left(-\hat{f}_{ij}\right) \tag{3.9}$$

$$B_{ij} = \mathrm{Re}\left(-\hat{f}_{ij}\right) \tag{3.10}$$

The radiation force can be analysed in the time domain by applying an inverse Fourier transform to Eq. (3.8). One classical property of the inverse Fourier transform is to convert the product of two functions in the frequency domain to the convolution of their inverse Fourier transforms (Riley et al., 2006). We obtain then

$$F_{kj}(\mathrm{t}) = \int_{-\infty}^{\infty} \widetilde{U}_j(\tau)\widetilde{f}_{kj}(t-\tau)d\tau \tag{3.11}$$

where the variables are now expressed as a function of time and the tilde stands for inverse Fourier transform. We should notice that, generally, the transfer function defined in Eq. (3.8) tends to a finite value as $\omega \to \infty$. Indeed, the added mass at infinite frequency defined in Eq. (3.2) is a

constant that can be separated from the frequency dependent part,

$$\hat{f}_{ij}(\omega) = -\mathrm{i}\omega\left(\bar{A}_{ij}(\omega) + A_{ij}^{\infty}\right) - B_{ij}(\omega) \tag{3.12}$$

where

$$\bar{A}_{ij}(\omega) = A_{ij}(\omega) - A_{ij}^{\infty} \tag{3.13}$$

Now the inverse Fourier transform of the RTF can be derived as

$$\widetilde{f}_{ij}(t) = \frac{1}{2\pi}\int_{-\infty}^{\infty}\left(-\mathrm{i}\omega\bar{A}_{ij}(\omega) - B_{ij}(\omega)\right)\mathrm{e}^{\mathrm{i}\omega t}d\omega - A_{ij}^{\infty}\dot{\delta}(t) \tag{3.14}$$

and defining

$$K_{ij}(t) = \frac{1}{2\pi}\int_{-\infty}^{\infty}\left(\mathrm{i}\omega\bar{A}_{ij}(\omega) + B_{ij}(\omega)\right)\mathrm{e}^{\mathrm{i}\omega t}d\omega \tag{3.15}$$

we derive an expression for the RIRF based on the inverse Fourier transform of the frequency-domain radiation parameters. Note that from this definition, it follows from Eqs (3.11), (3.14) that the radiation force can be described by:

$$F_{ij}(t) = -\int_{-\infty}^{\infty}\widetilde{U}_j(\tau)K_{ij}(t-\tau)d\tau - A_{ij}{}^{\infty}\dot{\widetilde{U}}_j(\tau) \tag{3.16}$$

The RIRF K_{ij} (also called retardation function or memory function) physically represents the effect of the past body oscillations on its actual state and is therefore real and causal, i.e. it obeys the relation

$$K_{ij}(t) = 0 \quad \text{for} \quad t < 0 \tag{3.17}$$

Then Eq. (3.16) can be modified to integrate up to time t only

$$F_{ij}(t) = -\int_{-\infty}^{t}\widetilde{U}_j(\tau)K_{ij}(t-\tau)d\tau - A_{ij}^{\infty}\dot{\widetilde{U}}_j(\tau) \tag{3.18}$$

The latter relation is perfectly analogous to the radiation terms we have introduced in the Cummins equation (3.1).

Note that Eq. (3.15) indicates that the RIRF can be defined as the inverse Fourier transform of the frequency-domain function $\hat{K}_{ij}(\omega)$, called here RTF and defined as:

$$\hat{K}_{ij}(\omega) = \mathrm{i}\omega\bar{A}_{ij}(\omega) + B_{ij}(\omega) \tag{3.19}$$

The fact that the RIRF is real can be interpreted as a consequence of the fact that $\hat{K}_{ij}(\omega)$ is Hermitian, i.e. its real part is an even function of ω and its imaginary part is odd. This implies that Eq. (3.15) can be written as:

$$K_{ij}(t) = \frac{1}{\pi}\int_{0}^{\infty}\left(-\omega\bar{A}_{ij}(\omega)\sin\omega t + B_{ij}(\omega)\cos\omega t\right)d\omega \tag{3.20}$$

We know from Chapter 2 that the added mass and the radiation damping coefficients are related by the Kramers–Kronig relations (Kotik and Mangulis, 1962). This implies the causality of the RIRF and also indicates that only the knowledge of either the radiation damping or of the added mass is required to derive it.

This can be inferred also by noting that, for the right-hand side of Eq. (3.20) to be identically zero when $t<0$, the following relation needs to apply:

$$-\int_{0}^{\infty}\omega\bar{A}_{ij}(\omega)\sin\omega t\,d\omega = \int_{0}^{\infty}B_{ij}(\omega)\cos\omega t\,d\omega \quad \text{for } t \neq 0 \tag{3.21}$$

So that the RIRF can be found by computing one of the following two integrals:

$$K_{ij}(t) = \frac{2}{\pi}\int_{0}^{\infty}B_{ij}(\omega)\cos\omega t\,d\omega \tag{3.22}$$

$$K_{ij}(t) = -\frac{2}{\pi}\int_{0}^{\infty}\omega\bar{A}_{ij}(\omega)\sin\omega t\,d\omega \tag{3.23}$$

Note that expressions (3.22) and (3.23) are applicable only for $t>0$. As mentioned earlier, for $t<0$, the RIRF is equal to zero. At $t=0$, there is a discontinuity because Eq. (3.20) imposes that

$$K_{ij}(0) = \frac{1}{\pi}\int_{0}^{\infty}B_{ij}(\omega)d\omega \tag{3.24}$$

even though the limit for $t \to 0^+$ given by Eq. (3.23) gives a value which is double that of Eq. (3.24).

The RIRF tends to 0 as $t \to +\infty$, as it follows from application of the Riemann–Lebesgue lemma to Eq. (3.22). This property ensures stability of the convolution term in Eq. (3.18) so that a bounded velocity input results in a bounded output (Perez and Fossen, 2008a).

As shown by Ogilvie (1964), these expressions have reciprocal forms that allow deriving the added mass and radiation damping from the RIRF:

$$B_{ij}(\omega) = \int_0^\infty K_{ij}(t) \cos \omega t \, dt \tag{3.25}$$

$$\bar{A}_{ij}(\omega) = -\frac{1}{\omega} \int_0^\infty K_{ij}(t) \sin \omega t \, dt \tag{3.26}$$

Note that Eq. (3.26) can be used to derive the value of the added mass at infinite frequency once the RIRF is computed from Eq. (3.22) and the added mass is known at N frequencies:

$$A_{ij}^\infty = \frac{1}{N} \sum_{n=1}^{N} \left(A_{ij}(\omega_n) + \frac{1}{\omega_n} \int_0^\infty K_{ij}(t) \sin \omega_n t \, dt \right) \tag{3.27}$$

In theory, the expression inside the series in Eq. (3.27) should give the same value regardless of the frequency but the mean is recommended here to minimize possible numerical inaccuracies.

3.4.2 Numerical Computation of the RIRF

The time-varying RIRF can be derived by a number of methods, including linear time-domain boundary element methods (BEM) codes like TiMIT (Korsmeyer et al., 1999) or ACHIL3D (Clément, 1995, 1999) or indirectly by first solving the linear problem in the frequency domain with the same tools outlined in the previous chapter and then using the computed frequency-dependent hydrodynamic coefficients in Eq. (3.15), (3.22) or (3.23).

We note that there are three different numerical approaches that can be applied for the computation of the RIRF from frequency-domain parameters:

I. Inverse Fourier transform of the RTF according to Eq. (3.15). This makes use of both the added mass and radiation damping coefficient.

II. Cosine transform of the radiation damping coefficient according to Eq. (3.22).

III. Sine transform of the added mass coefficient $\bar{A}_{ij}$ according to Eq. (3.23).

Theoretically, all these expressions are equivalent and should produce the same results. In practice, however, method II is preferred because it is less prone to numerical inaccuracies.

We note that the integrals in each of these equations should, in theory, be evaluated up to infinity so that one of the main sources of inaccuracies from the numerical integration comes from the need of either truncating the integral or extrapolating the hydrodynamic coefficients to infinite frequency.

Experience shows that, in most cases, the radiation damping tends to zero much faster than the added mass $\bar{A}_{ij}$ so that the error introduced by truncation or extrapolation is smaller if the computation of the RIRF is carried out following approach II. Furthermore, for those cases where the added mass at infinite frequency is unknown, method II is actually the only one that is directly applicable. Thus, we assume in the following that the RIRF is computed using the cosine transform of the radiation damping coefficient.

The integral in Eq. (3.28) is evaluated after truncation at a properly defined frequency. Since the radiation damping coefficient $B(\omega)$ tends asymptotically to zero as the frequency tends to infinity, it is sufficient to introduce an upper limit for this coefficient to be negligible. For instance, taking as the truncation frequency the one above which $B(\omega)$ is less than

one thousandth its maximum value produces satisfactory accuracy in most cases.

However, this is not always possible with commercial BEM codes since the largest frequency at which the coefficients are evaluated is limited by the number of panels (or, more correctly, the average panel size in comparison with the wave length) and the radiation damping coefficient might be still significant at the highest frequency assumed in the computation. Thus, in some cases extrapolation of the radiation coefficient to the highest frequencies is needed prior to the integration. This can be performed by either taking the value of the radiation damping equal to zero for a very high frequency and then use a cubic interpolant or by assuming that its high-frequency tail follows the rule

$$B_{ij}(\omega) \approx \frac{\alpha}{\omega^2} + \frac{\beta}{\omega^4} \tag{3.28}$$

as suggested by Greenhow (1986) and derived by Perez and Fossen (2008b). The coefficients α and β can then be determined by fitting the resulting curve to the descending section of the radiation damping coefficient.

Regardless of the extrapolation method used, a truncation is nevertheless applied. If we choose a frequency Ω sufficiently high so that the damping coefficient is very close to zero we can truncate the integral:

$$K_{ij}(t) = \frac{2}{\pi}\int_0^{\Omega} B_{ij}(\omega)\cos\omega t\, d\omega \tag{3.29}$$

The error resulting from this approximation is given by the remaining integral

$$\Delta = \frac{2}{\pi}\int_{\Omega}^{\infty} B_{ij}(\omega)\cos\omega t\, d\omega \tag{3.30}$$

which will be obviously close to zero as far as the damping coefficient is very small in the remaining frequency interval.

Sensitivity analysis can be performed on different truncation frequencies to check their influence on the value of the RIRF. Eq. (3.24) shows that the value of the RIRF at 0 is affected by the values of the radiation damping over the whole spectrum of frequencies, so a quick way to check the suitability of the truncation is to carry out this calculation and look for convergence to a fixed value. Poor numerical estimation due to unsuitable truncation is also revealed by the presence of a high-frequency tail in the RIRF for time tending to infinity. Alternatively, some authors (Kashiwagi, 2004; Armesto et al., 2015) suggest using an exponential for the extrapolation of the radiation damping so that the solution for the integral up to infinity in Eq. (3.30) can be derived analytically and any truncation error is avoided.

Integration of Eq. (3.29) is performed numerically often by applying conventional cumulative trapezoidal methods. The vector of values of the radiation damping coefficient is preliminarily interpolated over the required frequency range by using an evenly distributed frequency vector with specified frequency spacing. It should be noticed, however, that the integrand is a highly oscillating function, so that these methods might be particularly inaccurate when the oscillating frequency of the integrand is very high (typically higher than the inverse of the discretized integration step).

The use of conventional cumulative trapezoidal methods can produce a periodical function which can affect the subsequent solution of the body dynamics in the time domain if not properly handled. To avoid the occurrence of such errors, it is necessary to define the RIRF over a time span that is smaller than the inverse of half of the frequency spacing. Fig. 3.4 shows the RIRF computed with different frequency spacings for a cylinder whose radius and draught equal 5 m. Its decay is very quick and its contribution is practically negligible after a few tenths of seconds so that the RIRF is expected to be virtually equal to zero for $t > 30$ s.

However, if we chose to carry out the computation on a set of values defined over a frequency vector with spacing equal to 0.2 rad/s, we would find a peak around 30 s, as shown in Fig. 3.4. This occurrence is a purely numerical artefact and is due to the application of the trapezoidal method,

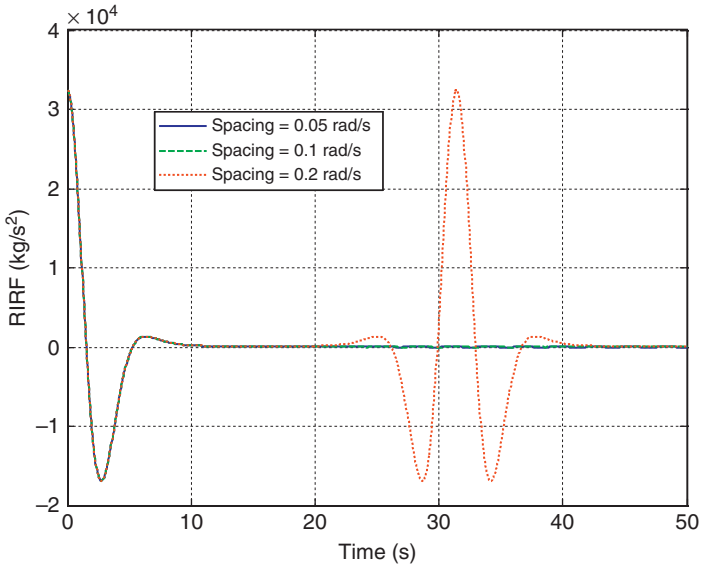

FIG. 3.4 RIRF in heave of a cylinder of radius and draught equal to 5 m computed with different frequency spacings.

which generates a periodic function with period equal to the inverse of the frequency spacing (in this case $T = 2\pi/0.2 = 31.42$ s).

In practice, because of its decaying behaviour, the RIRF only needs to be defined for the few first tens of seconds in the solution of time-domain models so, if proper frequency spacing is selected, no problems arise due to the periodicity of the function because it would appear much later (eg, for 0.05 rad/s spacing, the period is equal to 125.67 s). However, the decaying time for the RIRF is not always known prior to computation, particularly when complicated floating structures are modelled, so preliminary inspection and assessment of the RIRF behaviour is always recommended.

3.5 CONVOLUTION OF THE RADIATION FORCES

A major challenge in the solution of Eq. (3.1) is the calculation of the convolution integral. To solve Eq. (3.1) directly we need to find the solution of the convolution integral at every time instant, which is possible, once the RIRF is known, by performing a numerical integration along the previous time history. If we use classical ODE single-step numerical methods for the direct integration of the Cummins equation, this operation can be implemented inside the numerical algorithm but is computationally demanding, especially if many degrees of freedom are considered. Moreover, in many applications, such as control theory, a state-space representation is usually preferable since it is suited to many analysis tools used in automatic control.

Consequently, significant effort has been made to define solution methods that get rid of the convolution integral. All of these methods are characterized by the substitution of the convolution integral with an additional number of states, which increases the number of ODEs to be solved. Under broad categorization, convolution replacement methods can be grouped into two main types: time-domain identification and frequency-domain identification, depending on the input function used for deriving the equivalent state-space representation.

Time-domain identification was applied by Yu and Falnes (1996) to define a state-space model based on the approximation of the radiation convolution term with a determined number of linear subsystems by using a least-squares fitting of the RIRF. Such an approach proved to be quite accurate if the number of the states involved for the representation of the convolution term was large enough but consistently time-consuming if many geometries needed to be modelled. A variant for the time-domain fitting of the memory function relies on the use of the realization theory (Ho and Kalman, 1966; Kung, 1978) and has been introduced by Kristiansen and Egeland (2003) for modelling ship motions.

A very fast and efficient method for the state-space representation of the RIRF has been developed by the wave energy research team based in École Centrale de Nantes. This approach makes use of the Prony identification method (Clément, 1995; Duclos et al., 2001; Babarit et al., 2005) and can be classified as a time-domain identification method even though its theoretical basis is slightly different from the previous approaches.

Frequency-domain identification approximates the convolution term by means of a rational function in the frequency domain. This transfer function is fitted using the frequency-dependent hydrodynamic coefficients and subsequently transformed to the time domain by appropriate use of the Fourier transform. This approach was applied by Jefferys (1980, 1984), Damaren (2000), McCabe (2005) among others.

A comprehensive resume and comparison of these approaches has been recently offered by Taghipour et al. (2008) who showed the application of some of these methods to the case of a container ship. Comparisons of different methods for the case of wave energy conversion have been shown by Ricci et al. (2008), Kurniawan et al. (2011) and, more recently, Armesto et al. (2015). The following subsections describe the four main methods for calculating the convolution integral: namely, direct numerical integration, Prony identification method, time-domain identification and frequency-domain identification.

3.5.1 Direct Numerical Integration

As shown in Section 3.4, the RIRF is negligible after a relatively short time t_{decay} so the convolution integral can be computed by carrying out a numerical integration over the last t_{decay} instants of the time history of the body velocity.

$$\begin{aligned} I(t) &= \int_{-\infty}^{t} K_{ij}(t-\tau)\dot{x}_j(\tau)d\tau \\ &\cong \int_{t-t_{\text{decay}}}^{t} K_{ij}(t-\tau)\dot{x}_j(\tau)d\tau \end{aligned} \tag{3.31}$$

Using a cumulative trapezoidal method and assuming that the numerical method to solve the ODEs has constant time step Δt, the convolution integral can be written as:

$$\begin{aligned} I(t) \cong & \frac{K_{ij}(0)\dot{x}_j(t) + K_{ij}(t)\dot{x}_j\left(t-t_{\text{decay}}\right)}{2} \\ & + \sum_{m=1}^{N-1} K_{ij}(m\Delta t)\dot{x}_j(t-m\Delta t) \end{aligned} \tag{3.32}$$

where the number of values N to be stored for the computation of the convolution at each time step is given by

$$N = \frac{t_{\text{decay}}}{\Delta t} \tag{3.33}$$

This means that, at every time step, N data points corresponding to the previous values of the velocity have to be stored and used in $2N+1$ arithmetic operations (products and sums). This applies to every pair of degree of freedom 'ij' for which the RIRF is not negligible and the convolution integral needs to be computed.

For a system of six degrees of freedom with symmetry in the longitudinal axis, as many as 18 convolution terms are required with a total of $36(N+1)$ operations per time step. Clearly, if the time step is small (as might be required for

convergence and stability of the numerical method), the direct numerical integration of the convolution involves a large number of computations per time step, which severely affects the computational time required to find a solution.

3.5.2 Prony Identification Method

The Prony analysis was developed by Gaspard Riche, Baron de Prony in 1795 in order to explain the expansion of various gases. In his original paper (de Prony, 1795), Prony proposed fitting a sum of exponentials to equally spaced data points and extended the model to interpolate at intermediate points. The Prony identification method approximates the convolution integral by representing the RIRF as a sum of N exponentials with complex coefficients and exponents:

$$K_{ij}(t) \cong \sum_{k=1}^{N} \alpha_k e^{\beta_k t} \tag{3.34}$$

This allows interpreting the convolution integral as the sum of N integrals:

$$I(t) = \sum_{k=1}^{N} \int_0^t \alpha_k e^{\beta_k (t-\tau)} \dot{x}_j(\tau) d\tau = \sum_{k=1}^{N} I_k(t) \tag{3.35}$$

$$\dot{I}_k(t) = \alpha_k \dot{x}_j(\tau) + \beta_k I_k(t) \tag{3.36}$$

Since the function is known at evenly spaced points $t_m = m\Delta t$, then, at each point we can write

$$K_{ij}(t_m) = \alpha_1 V_1^m + \alpha_2 V_2^m + \cdots + \alpha_N V_N^m \tag{3.37}$$

where $V_k = e^{\beta_k \Delta t}$. Considering the polynomial $P_N(z)$ given by the equation:

$$P_N(z) = \prod_{p=1}^{N} (z - V_p) = \sum_{p=0}^{N} s_p z^{N-p} \tag{3.38}$$

where the exponentials V_k are roots of the polynomial and $s_0 = 1$. Then, it can be shown that the following expression holds:

$$\sum_{p=0}^{N} s_{N-p} K_{ij}(t_p) = \sum_{k=1}^{N} \alpha_k P_N(V_k) \tag{3.39}$$

Since $P_N(V_k) = 0$ and $s_0 = 1$, this reduces to:

$$\sum_{p=0}^{N-1} s_{N-p} K_{ij}(t_p) = -K_{ij}(t_N) \tag{3.40}$$

Eq. (3.40) has N unknowns (the coefficients s_{N-p}) and is based on $N+1$ values of the RIRF sampled over an array of evenly spaced time instants.

The starting point ($p = 0$) of this expression can be 'shifted' to the subsequent value to generate another equation for the same unknown coefficients. By repeating M times this 'shifting', a linear system of $M \geq N$ equations can be derived:

$$\begin{cases} \sum_{p=0}^{N-1} S_{N-p} K_{ij}(t_p) = -K_{ij}(t_N) \\ \sum_{p=1}^{N} S_{N-p} K_{ij}(t_p) = -K_{ij}(t_{N+1}) \\ \qquad \cdots = \cdots \\ \sum_{p=M}^{N+M-1} S_{N-p} K_{ij}(t_p) = -K_{ij}(t_{N+M}) \end{cases} \tag{3.41}$$

To obtain a solution for the polynomial coefficients, at least $2N+1$ values of the RIRF have to be defined. In this case, the matrix of the system is square and gives a unique solution. If $M > N$, the previous system is overdetermined and can be solved by standard least squares methods.

Once the coefficients s_p are known, the roots V_k of the polynomial can be found by any root-finding algorithm. The exponents β_k are then derived by

$$\beta_k = \frac{\ln V_k}{\Delta t} \tag{3.42}$$

Using Eq. (3.37), another overdetermined linear system can be built to obtain the coefficients α_k:

$$\begin{cases} \alpha_1 + \alpha_2 + \cdots + \alpha_N = K_{ij}(t_0) \\ \alpha_1 V_1 + \alpha_2 V_2 + \cdots + \alpha_N V_N = K_{ij}(t_1) \\ \alpha_1 V_1^2 + \alpha_2 V_2^2 + \cdots + \alpha_N V_N^2 = K_{ij}(t_2) \\ \qquad \cdots = \cdots \\ \alpha_1 V_1^{N+M} + \alpha_2 V_2^{N+M} + \cdots + \alpha_N V_N^{N+M} = K_{ij}(t_{N+M}) \end{cases} \tag{3.43}$$

The resulting coefficients α_k and exponents β_k can be used in Eqs (3.35), (3.36) to yield a state-space model where each integral $I_k(t)$ can be considered a state variable. The number of exponentials is defined by the desired accuracy. This can be controlled automatically by checking the relative error of the Prony approximation (3.34) with respect to the computed RIRF.

The effect of the number of exponentials in the accuracy of the RIRF identification is shown in Fig. 3.5 for the case of a cylinder with radius and draught equal to 5 m. Using five exponentials can produce significant errors in this case in the first instance. However, increasing the number of exponentials up to seven is already sufficient to yield a very good fitting. Note that all cases show practically the same response at $t > 7$ s. It is often the case that the large oscillations of the RIRF in the first few seconds are the most difficult to fit.

The Prony approximation typically delivers exponents β_k which are either real or complex conjugate in pairs. The real part of the exponent should always be negative, otherwise the exponential would tend to infinity for $t \to \infty$ and the whole time-domain model would become unstable. For this reason, the coefficients derived by Prony identification should be filtered prior to their implementation in the time-domain solver to remove possible exponents with positive real parts.

Since the exponents are either real or complex conjugate pairs, the convolution integral as a result of the sum of the integrals in Eq. (3.35) should always be real. Nevertheless, numerical errors, particularly when a small number of exponentials are used, can produce small imaginary parts in the evaluation of the convolution. These should be ignored by the solver since the convolution integral used in the solution of the Cummins equation is always real.

3.5.3 Time-Domain Identification

The identification of the convolution integral in the time domain can be carried out by applying a variety of approaches. The common aspect of all of them is that they build a state-space

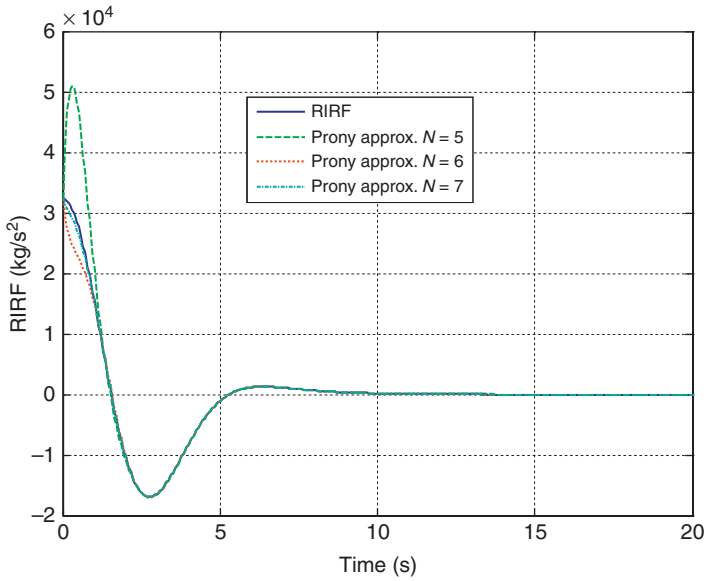

FIG. 3.5 RIRF in heave of a cylinder of radius and draught equal to 5 m and corresponding approximation by Prony's method using different numbers of exponentials.

model for the convolution integral that has the following form:

$$I(t) = \sum_{k=1}^{N} C_k I_k(t) + D\dot{x}_j(t) \tag{3.44}$$

$$\dot{I}_k(t) = \sum_{n=1}^{N} A_{kn} I_n(t) + B_k \dot{x}_j(t) \tag{3.45}$$

where A is a matrix and B, C, and D are vectors defined by the identification procedure. $I(t)$ is the convolution integral defined earlier in Eq. (3.31).

In practice, N differential equations formulated as in Eq. (3.45) are added to the system, similarly to what was shown for the Prony approach. Indeed, we can see that Eqs (3.35), (3.36) can be considered as a variant of Eqs (3.44), (3.45), where A is the identity matrix with the diagonal terms given by the β_k coefficients, $B_k = \alpha_k$, C is a vector whose elements are all 1 and $D = 0$.

The system-identification problem for state-space systems is sometimes called the 'realization problem'. That is, we wish to find a realization (a set of A, B, C, and D matrices) that describes a system's dynamics. Many possible realizations of the state-space model exist. They are all based on analytical decompositions or optimization procedures to identify the coefficients of A, B, C, and D that deliver the best fit. However, the numerical procedures to produce them are different and so are the results.

Yu and Falnes (1996) applied the so-called companion form realization, which assumes that the matrix A and the vectors B and C have the following form:

$$A = \begin{bmatrix} 0 & 0 & \dots & 0 & 0 & -a_1 \\ 1 & 0 & \dots & 0 & 0 & -a_2 \\ 0 & 1 & \dots & 0 & 0 & -a_3 \\ \dots & \dots & \dots & \dots & \dots & \dots \\ 0 & 0 & \dots & 1 & 0 & -a_{N-1} \\ 0 & 0 & \dots & 0 & 1 & -a_N \end{bmatrix} \tag{3.46}$$

$$B = [b_1 \;\; b_2 \;\; b_3 \;\; \dots \;\; b_{N-1} \;\; b_N] \tag{3.47}$$

$$C = [0 \;\; 0 \;\; 0 \;\; \dots \;\; 0 \;\; 1] \tag{3.48}$$

Assuming that $D = 0$ and that the velocity input $\dot{x}_j(t)$ is causal (it is 0 as $t < 0$), the RIRF can be approximated by the expression:

$$K_{ij}(t) \cong C e^{At} B^T \tag{3.49}$$

where the term e^{At} is the matrix exponential, an operator applicable to square matrices and defined as

$$e^{At} = \sum_{r=0}^{\infty} \frac{1}{r!} A^r t^r \tag{3.50}$$

The matrix exponential produces an $N \times N$ matrix, the same size of A.

Thus, once the order of the system N is selected, a total of $2N$ parameters have to be defined to characterize completely the matrix A and the vector B. These unknown parameters are described as the elements of the vector ε:

$$\varepsilon = [a_1 \;\; a_2 \;\; \dots \;\; a_N \;\; b_1 \;\; b_2 \;\; \dots \;\; b_N] \tag{3.51}$$

The approach then relies on the minimization of the error function given by the difference between the RIRF and the approximation in Eq. (3.49). This can be expressed by the following relation:

$$\varepsilon_{\text{opt}} = \arg\min_{\varepsilon} \sum_{p=1}^{M} w(t_p) \times \left(K_{ij}(t_p) - \sum_{n=1}^{N} \left(e^{A(\varepsilon) t_p} \right)_{Nn} b_n(\varepsilon) \right)^2 \tag{3.52}$$

where the vector ε_{opt} represents the set of parameters derived by minimizing the fitting error over an array of M chosen time instants for which the RIRF is known. The error function on the right-hand side can contain a properly defined weight function $w(t_p)$ which can be used, for example, to enforce better fitting at those points where the RIRF is large (typically the first few seconds).

Eq. (3.52) represents a typical optimization problem, nonlinear in the parameters ε, which can be solved by Levenberg–Marquardt or Gauss–Newton algorithms (Bazaraa et al., 2006). Any of these methods require an initial guess for ε. The number of parameters to solve can be further reduced by noticing that

$$b_N = K_{ij}(0^+) \tag{3.53}$$

Thus, in total $2N-1$ parameters are effectively required to build the state-space system in Eqs (3.44), (3.45). One of the advantages of this approach is that the number of parameters is independent of the number of sampled values available for the RIRF. Furthermore, it does not require the time instants to be evenly spaced so that no preliminary treatment of the RIRF is needed and the identification can be carried out on a very small number of time instants.

However, the selection of the initial guess has an important effect on the computational time and on the quality of the results as the number of iterations required to converge to a solution to the optimization problem given by Eq. (3.52) is variable depending on the starting point. Furthermore, the cost-function given in Eq. (3.52) is rarely convex so that the algorithm could identify local minima associated with very large residuals. A simple initial estimate for the parameters can be provided by assuming they are all equal to 1. For simple geometries, this appears to work well but the fitting can be very poor for more complicated structures.

A significant drawback of this technique is the absence of control on the behaviour of the fitted function. No assumptions are made on the properties and form of the matrix A, which, at times, can be found to have eigenvalues with positive real part. This has the consequence of generating numerical instability in the solution of the time-domain model because the fitted RIRF tends to diverge as the time increases. Because the procedure shown previously is purely numerical, there is no straightforward method that allows filtering of the parameters to produce a stable solution and the user is required to carry out further optimizations, possibly with different initial guesses, until a stable solution is found.

In principle, an increase in the number N of additional states should improve the accuracy of the fit, provided that the stability of the system is ensured. However, when a large number of states (eg, larger than six) is considered, there is high probability that the optimization algorithm will produce an unstable solution.

Fig. 3.6 shows the application of this technique to the case of a cylinder with radius and draught equal to 5 m. In this case, the improvement of the fitting due to an increase in the number of states is clear.

Fig. 3.6 also shows the influence of the introduction of a vector of weights to ensure better fitting at some specific points. A vector of weights, whose definition was based on the absolute value of the RIRF, has been applied in the identification process of the straight purple line and of the dotted yellow line. The error with respect to the RIRF for times larger than 5 s is much larger than for the other curves, which were identified without considering any weight. This happens because the absolute value of the RIRF at these instants is relatively small compared to the values in the first time instants. Thus, the introduction of a weight vector proportional to the absolute value of the RIRF ensures better fitting at the first time instants but performs slightly worse in the remaining of the time history.

An alternative time-domain identification state-space realization method was introduced by Ho and Kalman (1966) and is based on the direct derivation of the state-space parameters from the samples of the impulse response. The Ho–Kalman method is usually applied to a discrete-time system of the type:

$$\begin{cases} x(k+1) = A_{\mathrm{d}}x(k) + B_{\mathrm{d}}u(k) \\ y(k) = C_{\mathrm{d}}x(k) + D_{\mathrm{d}}u(k) \end{cases} \tag{3.54}$$

The impulse response of a discrete state-space system, defined as the response to a unit pulse, is then found as

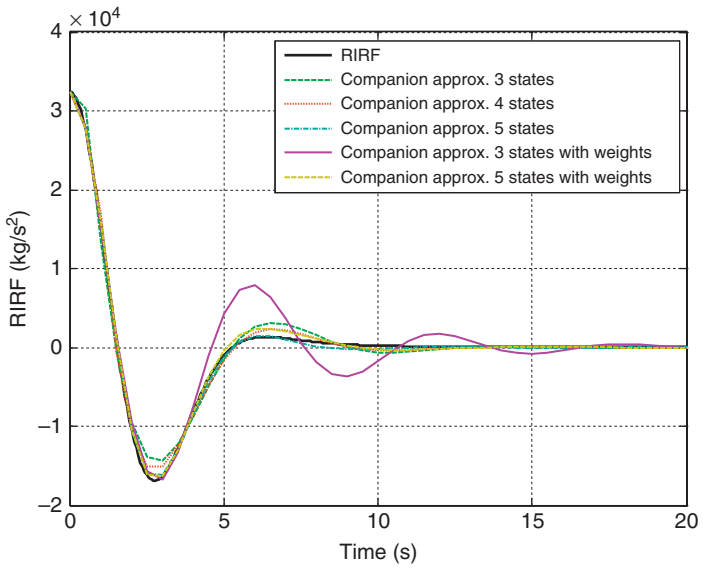

FIG. 3.6 RIRF in heave of a cylinder of radius and draught equal to 5 m and corresponding approximation by time-identification method based on the companion form using a different number of states.

$$K_{\mathrm{d}}(k) = \begin{cases} D_{\mathrm{d}} & k = 0 \\ C_{\mathrm{d}} A_{\mathrm{d}}^{k-1} B_{\mathrm{d}} & k > 0 \end{cases} \tag{3.55}$$

These unit-pulse response values $\{D_{\mathrm{d}}, C_{\mathrm{d}}B_{\mathrm{d}}, C_{\mathrm{d}}A_{\mathrm{d}}B_{\mathrm{d}}, C_{\mathrm{d}}A_{\mathrm{d}}^2B_{\mathrm{d}}, \ldots\}$ are called the Markov parameters of the system and are the basis for the definition of the following Hankel matrix $\mathcal{H}$:

$$\mathcal{H} = \begin{bmatrix} C_{\mathrm{d}}B_{\mathrm{d}} & C_{\mathrm{d}}A_{\mathrm{d}}B_{\mathrm{d}} & C_{\mathrm{d}}A_{\mathrm{d}}^2B_{\mathrm{d}} & \ldots & C_{\mathrm{d}}A_{\mathrm{d}}^{n-1}B_{\mathrm{d}} \\ C_{\mathrm{d}}A_{\mathrm{d}}B_{\mathrm{d}} & C_{\mathrm{d}}A_{\mathrm{d}}^2B_{\mathrm{d}} & C_{\mathrm{d}}A_{\mathrm{d}}^3B_{\mathrm{d}} & & \\ C_{\mathrm{d}}A_{\mathrm{d}}^2B_{\mathrm{d}} & C_{\mathrm{d}}A_{\mathrm{d}}^3B_{\mathrm{d}} & C_{\mathrm{d}}A_{\mathrm{d}}^4B_{\mathrm{d}} & & \\ \vdots & & & \ddots & \vdots \\ C_{\mathrm{d}}A_{\mathrm{d}}^{n-1}B_{\mathrm{d}} & & & \ldots & C_{\mathrm{d}}A_{\mathrm{d}}^{2n-2}B_{\mathrm{d}} \end{bmatrix} \tag{3.56}$$

For any state-space system described by Eq. (3.54), the observability matrix $\mathcal{O}$ is the tuple given by

$$\mathcal{O} = \begin{bmatrix} C_{\mathrm{d}} \\ C_{\mathrm{d}}A_{\mathrm{d}} \\ C_{\mathrm{d}}A_{\mathrm{d}}^2 \\ \vdots \\ C_{\mathrm{d}}A_{\mathrm{d}}^{n-1} \end{bmatrix} \tag{3.57}$$

whereas the controllability matrix $\mathcal{C}$ is defined as

$$\mathcal{C} = \begin{bmatrix} B_{\mathrm{d}} & A_{\mathrm{d}}B_{\mathrm{d}} & A_{\mathrm{d}}^2B_{\mathrm{d}} & \ldots & A_{\mathrm{d}}^{n-1}B_{\mathrm{d}} \end{bmatrix} \tag{3.58}$$

Knowledge of the controllability and observability matrices allows straightforward determination of the matrices B_{d} and C_{d} and, by inversion, of the matrix A_{d}.

It is seen that the Hankel matrix from Eq. (3.56) is the product between the observability and the controllability matrices $\mathcal{H} = \mathcal{O}\mathcal{C}$. Therefore, if a method is applicable to decompose the Hankel matrix $\mathcal{H}$ in such a way that $\mathcal{O}$ and $\mathcal{C}$ can be determined, all the parameters of the state-space system can be established. One such method is the singular value decomposition (SVD), which states that any rectangular matrix $M \in \mathbb{R}^{m \times n}$ with rank equal to r can be factored into the form:

$$M = U\Sigma V^{\mathrm{T}} \tag{3.59}$$

where $U \in \mathbb{R}^{m \times r}$, $V \in \mathbb{R}^{n \times r}$, and $U^{\mathrm{T}}U = V^{\mathrm{T}}V = I$. The matrix Σ is a diagonal matrix, with its diagonal given by the r singular values of M in descending order.

Being defined by the rank of the matrix M, the number of nonzero singular values can be very large. For instance, when the Hankel matrix is formed from the values of the impulse response given in Eq. (3.55), its rank is possibly as high as the number of values n defined from the computation of the RIRF. Since the main objective of this application is to construct a low-order state-space realization, it is often better to make a good low-order approximation of the RIRF rather than to try to match it exactly by using a very large number of states.

Because the singular values are given in descending order, it is possible to partition the matrices in Eq. (3.59), in such a way that only a reduced number of singular values is considered in the system representation. In practice, this is done by checking the magnitude of the singular values and deciding a specific threshold below which they can be neglected.

The SVD matrices can be factored then as:

$$M = [U_1 \;\; U_2] \begin{bmatrix} \Sigma_1 & 0 \\ 0 & \Sigma_2 \end{bmatrix} \begin{bmatrix} V_1 \\ V_2 \end{bmatrix} \tag{3.60}$$

where Σ_1 contains the most significant singular values, selected according to the specified threshold.

Thus, the Hankel matrix defined in Eq. (3.56) can be decomposed using the SVD procedure into:

$$\mathcal{H} = U_1 \Sigma_1 V_1^{\mathrm{T}} = U_1 {\Sigma_1}^{1/2} {\Sigma_1}^{1/2} V_1^{\mathrm{T}} \tag{3.61}$$

The last expression on the right-hand side allows defining the observability and controllability matrices as:

$$\mathcal{O} = U_1 {\Sigma}^{1/2} \tag{3.62}$$

$$\mathcal{C} = {\Sigma}^{1/2} V^{\mathrm{T}} \tag{3.63}$$

Therefore, we can extract B_{d} from the first column of the controllability matrix and C_{d} from the first row of the observability matrix:

$$B_{\mathrm{d}} = {\Sigma}^{1/2} V_{1,1:n}^{\mathrm{T}} \tag{3.64}$$

$$C_{\mathrm{d}} = U_{1,1:n} {\Sigma}^{1/2} \tag{3.65}$$

For the definition of the matrix A_{d}, we notice first that, by shifting the Hankel matrix by one block row, we obtain:

$$\mathcal{H}_s = \begin{bmatrix} C_{\mathrm{d}}A_{\mathrm{d}}B_{\mathrm{d}} & C_{\mathrm{d}}A_{\mathrm{d}}^2B_{\mathrm{d}} & \dots & C_{\mathrm{d}}A_{\mathrm{d}}^nB_{\mathrm{d}} \\ C_{\mathrm{d}}A_{\mathrm{d}}^2B_{\mathrm{d}} & C_{\mathrm{d}}A_{\mathrm{d}}^3B_{\mathrm{d}} & & \vdots \\ \vdots & & \ddots & \vdots \\ C_{\mathrm{d}}A_{\mathrm{d}}^{n-1}B_{\mathrm{d}} & & \dots & C_{\mathrm{d}}A_{\mathrm{d}}^{2n-2}B_{\mathrm{d}} \\ C_{\mathrm{d}}A_{\mathrm{d}}^nB_{\mathrm{d}} & \dots & \dots & C_{\mathrm{d}}A_{\mathrm{d}}^{2n-1}B_{\mathrm{d}} \end{bmatrix} = \mathcal{O}A_{\mathrm{d}}\,\mathcal{C} = U_2\Sigma_1 V_1^T \tag{3.66}$$

where U_2 is the matrix obtained by shifting U_1 by one block row.

Therefore, the matrix A_{d} can be found by the expression

$$A_{\mathrm{d}} = \mathcal{O}^{-1} U_2 \Sigma_1 V_1^T \mathcal{C}^{-1} \tag{3.67}$$

where the M^{-1} operator stands for the pseudo-inverse of matrix M, since the observability and controllability matrices are, in general, not square.

By substitution of Eqs (3.62), (3.63) into Eq. (3.67), we find, for A_{d}:

$$A_{\mathrm{d}} = {\Sigma}^{1/2} U_1 U_2 {\Sigma}^{1/2} \tag{3.68}$$

Finally, D_{d} is simply given by the value of the impulse response at the first instant:

$$D_{\mathrm{d}} = K_{\mathrm{d}}(0) \tag{3.69}$$

The set of parameters A_{d}, B_{d}, C_{d}, and D_{d} describe a discrete state-space representation of an impulse response sampled at a discrete number of time instants. However, continuous representations are required for the solution of the time-domain system (Eq. 3.1), because all the formulations and numerical methods introduced earlier operate on the continuous time history. Therefore, the discrete state-space system (A_{d}, B_{d}, C_{d}, D_{d}) is converted into the continuous state-space system (A, B, C, D) by applying the bilinear transformation, also known as Tustin's method (Al-Saggaf and Franklin, 1987).

The values of the impulse response used for the construction of the Hankel matrix need to

be scaled from the continuous-time version of the RIRF defined in the previous section:

$$K_d(t_k) \approx T_s \cdot K(t_k) \tag{3.70}$$

where T_s is the selected sampling time, greater than or equal to the time step used for the computation of the RIRF in Section 3.4.2, ie, $T_s \geq \Delta t$.

The whole procedure for the state-space identification following the Ho and Kalman realization theory can therefore be summarized by the following steps:

- Sample the RIRF at discrete time instants t_k defined as $t_k = kT_s$. To avoid the need for interpolation, choose a sampling time T_s which is a multiple of the original time step Δt used for the calculation.
- Define the discrete unit-pulse response by applying the scaling according to Eq. (3.70).
- Form the Hankel matrix, using the sampled values of the discrete unit-pulse response, as from Eq. (3.56).
- Carry out the SVD on the Hankel matrix and select the most significant singular values, according to a predefined threshold.
- Decompose the matrices found from the application of the SVD to obtain U_1, Σ_1, and V_1 as per Eq. (3.61).
- Construct the discrete state-space matrices A_d, B_d, C_d, and D_d by applying Eqs (3.64), (3.65), (3.67), and (3.69).
- Convert the discrete state-space system to the continuous time by using the Tustin transform (Al-Saggaf and Franklin, 1987)

An implementation of the algorithm is already available in Matlab in the function *imp2ss* of the Robust Control Toolbox. Application of the realization theory to the time-domain analysis of offshore structures has been shown by Kristiansen and Egeland (2003) and has been applied by other authors (Taghipour et al., 2008; Perez and Fossen, 2008a; Ricci et al., 2008).

Under this approach, the order of the system is determined by the number of singular values retained after the application of the predefined threshold. Although this ensures a good accuracy, the number of states required for a satisfactory representation may be very large, particularly if the chosen sampling time is small.

Kristiansen et al. (2005) show that the order of the model can be controlled directly by application of the truncated balanced reduction method to the state-space realization derived following the Ho and Kalman procedure. This allows obtaining low-order state-space representations that maintain almost the same accuracy and stability properties of the original realization. The truncated balanced reduction is also implemented in the Matlab routine *balancmr* of the Robust Control Toolbox and can be used to directly specify the desired order of the model.

Fig. 3.7 shows the RIRF of a cylinder with radius and draught equal to 5 m together with the estimated values provided by the realization method for different model orders. The quality of the fit is already very good for realizations of 4 states or higher. However, the initial value of the RIRF (ie, at $t = 0^+$) is not predicted correctly in any case. This is a typical limitation of this method, because of the properties of the discrete representation and the need for discrete-to-continuous transformation.

For instance, since the transfer function has a zero at $\omega = 0$, it is known that the constant D in Eq. (3.44) should be zero (Perez and Fossen, 2008a). However, the realization method always produces a nonzero D, because of its relation to the discrete state-space domain, where this constant is equal to the first value of the unit-pulse response. On the other hand, this method is very efficient in automated calculations since it does not require any initial guess and can be implemented in such a way that the additional number of states is established at the beginning. Furthermore, it generally produces very stable realizations. Although no theoretical reference was found to give details on the stability properties of the matrix generated by the Ho and Kalman algorithm, repeated application of this method on a number of different functions, in some cases even exponentially diverging with time, has shown that the numerical

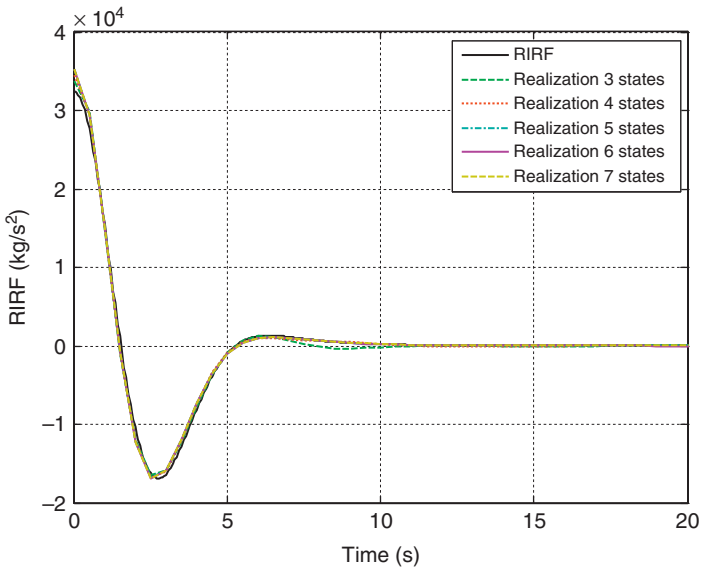

FIG. 3.7 RIRF in heave of a cylinder of radius and draught equal to 5 m and corresponding approximation by time-identification method based on the Ho and Kalman (1966) realization theory using a different number of states.

implementation provided by Matlab always produces a stable system. This might be related to the way the Hankel matrix is built, because the Matlab formulation pads the rows of the Hankel matrix with zeros after all the values given for the impulse response have been introduced.

The use of the Matlab toolbox is not the only available option. Some routines have been developed also for Python and other languages. However, the numerical implementation of the Ho and Kalman method can be difficult, particularly on the requirement for an efficient solver for the SVD, and can demand a significant programming effort.

3.5.4 Frequency-Domain Identification

All the methods introduced so far are based on the preliminary computation of the RIRF in the time domain, following the procedure presented in Section 3.4.2. As shown earlier, this computation can be time-consuming and is prone to errors arising from a poor truncation of the integral or from the selection of an unsuitable frequency step. This passage can be avoided if the operation of substituting the convolution integral is carried out in the frequency domain so that the hydrodynamic coefficients provided by panel codes can be used directly. Some preprocessing is nevertheless required, in particular on what concerns the extrapolation to high frequencies, but the intermediate step of generating the RIRF is avoided. Different approaches have been proposed in the literature following this idea but virtually all of them are characterized by the attempt of fitting a rational transfer function to the hydrodynamic coefficients found in the frequency domain.

Although this procedure can be performed on the complex added mass (Sutulo and Guedes Soares, 2005), it is customary to apply the fitting to the RTF introduced in Eq. (3.19). The RTF can be expressed as a function of the Laplace coordinate $s = i\omega$ as:

$$K_{ij}(s) = K_{ij}(\mathrm{i}\omega) = \hat{K}_{ij}(\omega) = \mathrm{i}\omega\bar{A}_{ij}(\omega) + B_{ij}(\omega) \tag{3.71}$$

The frequency-domain identification method consists of finding the polynomial coefficients b_m, b_{m-1}, … b_0 and a_{n-1}, … a_0 that allow representing the RTF as a rational function:

$$K_{ij}(s)=\frac{N(s)}{D(s)}=\frac{b_m s^m+b_{m-1}s^{m-1}+\cdots+b_1 s+b_0}{s^n+a_{n-1}s^{n-1}+\cdots+a_1 s+a_0} \tag{3.72}$$

By defining a vector of parameters

$$\varepsilon=[a_0\ \ a_1\ \ \ldots\ \ a_{n-1}\ \ b_0\ \ b_1\ \ \ldots\ \ b_m] \tag{3.73}$$

the corresponding optimization problem can be solved using the least-squares approach:

$$\varepsilon_{\text{opt}}=\arg\min_{\varepsilon}\sum_{p=1}^{n+m+1} w(\mathrm{s}_p)\left|K_{ij}(\mathrm{s}_p)-\frac{N(\mathrm{s}_p,\varepsilon)}{D(\mathrm{s}_p,\varepsilon)}\right|^2 \tag{3.74}$$

where $w(\mathrm{s}_p)$ is a vector of weights that can be introduced to enforce a better fitting at specified frequencies.

The preceding problem is nonlinear in the vector of parameters ε and can be solved by applying the damped Gauss–Newton method. Alternatively, a linear version can be devised by substituting the weight function with the square of the modulus of the denominator of the rational function:

$$w(\mathrm{s}_p)=|D(\mathrm{s}_p,\varepsilon)|^2 \tag{3.75}$$

This substitution turns the optimization problem of Eq. (3.74) into the linear problem:

$$\varepsilon_{\text{opt}}=\arg\min_{\varepsilon}\sum_{p=1}^{n+m+1}\frac{1}{|D(\mathrm{s}_p,\varepsilon_{k-1})|^2}|D(\mathrm{s}_p,\varepsilon)\times K_{ij}(\mathrm{s}_p)-N(\mathrm{s}_p,\varepsilon)|^2 \tag{3.76}$$

where a weight vector derived by the denominator calculated in the previous iteration has been introduced in such a way that an iterative procedure can be applied to estimate the vector of parameters ε.

Unfortunately, the numerical solution of Eq. (3.74) or (3.76) does not necessarily correspond to a stable system. The stability of a system is related to the position of the poles of its transfer function (ie, the values of s for which the denominator is equal to zero): if all the poles have negative real part, then the system is stable. However, one simple way of obtaining a stable identification consists of reflecting, with respect to the imaginary axis, the poles with positive real part. In practise this can be done by computing the roots corresponding to the polynomial coefficients of the denominator, reflecting any root with positive real part and recomputing the coefficients from the new roots.

Once the polynomial coefficients of the numerator and denominator have been established, the state-space formulation of the convolution integral can be retrieved by applying the canonical form:

$$A=\begin{bmatrix}-a_{n-1} & -a_{n-2} & \cdots & -a_1 & -a_0\\ 1 & 0 & \cdots & 0 & 0\\ 0 & 1 & \ldots & 0 & 0\\ \vdots & \vdots & \ddots & \vdots & \vdots\\ 0 & 0 & \cdots & 1 & 0\end{bmatrix} \tag{3.77}$$

$$B=\begin{bmatrix}1\\0\\\vdots\\0\\0\end{bmatrix} \tag{3.78}$$

$$C=[b_m\ \ b_{m-1}\ \ \cdots\ \ b_1\ \ b_0\ \ 0] \tag{3.79}$$

$$D=0 \tag{3.80}$$

where use is made of the knowledge that the transfer function has relative degree equal to 1 (ie, $n-m=1$) and that it is zero for $\omega=0$.

The Matlab function *invfreqs* of the Signal Processing Toolbox can be used to provide a solution to either Eq. (3.74) or (3.76). Additionally, the Marine Systems Simulator, a Matlab toolbox specifically developed for the frequency-domain identification of the radiation forces of offshore structures, has been developed by Perez and Fossen (2009) and can be found at http://www.marinecontrol.org/.

The frequency-domain identification method has been applied by Damaren (2000), McCabe et al. (2005) to the modelling of WECs and has been used since by many other modellers in the field. Considering the wide availability of codes for the computation of the rational function, its application is relatively straightforward. Furthermore, as mentioned earlier, the stability of the solution can be controlled and implemented automatically. Perez and Fossen (2011) have also shown that the efficiency of the method can be improved by applying the knowledge related to some properties of the RTF. For instance, since the RTF is zero at zero frequency, then the minimum order of the model is two and the identification process can begin with $n=2$ and proceed to increasing the model order until a satisfactory accuracy is achieved.

A comparison of the IRFs estimated by the FDI applying a different number of additional states is shown in Fig. 3.8 for the case of a cylinder of radius and draught equal to 5 m. The fitting is already quite good for $n=4$, though the introduction of an additional state ($n=5$) matches almost perfectly with the original RIRF, even for $t=0^+$. As it has been reported by Taghipour et al. (2008), increasing the order of the model does not necessarily determine an improvement in the accuracy of the solution, in particular if the number of additional states is already large.

3.6 HYDROSTATIC FORCES

The hydrostatic forces in the Cummins equation are the forces on a body due to change in hydrostatic pressure on the wetted surface of the body as it moves from its equilibrium position. Consequently, the hydrostatic forces are a function of the body displacements x_j. For small amplitudes of motion the hydrostatic forces are simple linear functions of the displacements, which can be defined by a matrix of stiffness

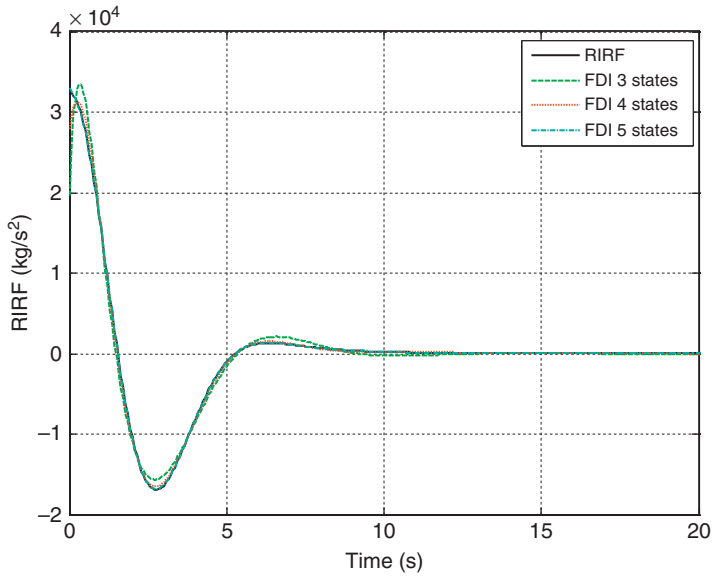

FIG. 3.8 RIRF in heave of a cylinder of radius and draught equal to 5 m and corresponding approximation by frequency-domain identification method using a different number of states.

coefficients. This is the standard approach for modelling WECs; however, for large amplitudes of motion and particularly where the body surface at the water-plane is not vertical then a nonlinear representation of the hydrostatic forces is more appropriate.

Although an analytical or semiempirical representation of the hydrostatic forces can sometimes be produced, in many cases it is easier to use a numerical integration of the hydrostatic pressure over the wetted surface of the body for a range of displacements to produce a look-up table that can be used in the time-domain model.

3.7 SOLUTION OF THE CUMMINS EQUATION

Once the convolution integral is transformed into a linear form, the Cummins equation (Eq. 1.1) can be easily solved by efficient prebuilt numerical routines usually available in many commercial packages (Matlab) or in publicly available libraries for open source languages (Octave, Python, Fortran). The most computationally efficient types of routines use a variable-step solver, where the time-step length ensures the errors are acceptable. The most commonly used variable-step solver is the Dormand–Prince fourth- and fifth-order Runge–Kutta solver; however, other solvers are available that are more suitable for particular cases, e.g. very stiff systems.

Where the convolution integral is represented using an increase in the order of state-space model (i.e. using a Prony, time-domain or frequency-domain identification method) then the use of a variable-step solver presents no problems. Application of variable-time step solvers is also theoretically possible for the direct numerical integral of the convolution integral but would require reevaluation and/or interpolation of the RIRF at those points for which values were not stored (since the time step used by the solver is not known in advance). Consequently, for direct numerical integration of the convolution integral a constant time step is typically more suitable (although variable-step solvers could be used, any benefit gained from reducing the computational time is likely to be offset by the need of additional evaluation of the RIRF).

Some examples of fixed-step solvers are (Conte and De Boor, 1980):

- Backward Euler
- Crank–Nicolson
- fourth-order Runge–Kutta
- Predictor–Corrector pair: Adams–Bashforth first order and Adams–Moulton second order
- Predictor–Corrector pair: Adams–Bashforth second order and Adams–Moulton third order

Implicit or semiimplicit methods derive the solution by applying iterative calculations within the same time step. Strict application of these methods would require the convolution integral to be updated in each iteration. This would be time-consuming and can be avoided by assuming that the estimation of the convolution integral is only based on the information from the previous step. Experience shows that, if the time step is sufficiently small, the error is negligible.

3.8 CASE-STUDY: A SINGLE-BODY HEAVING WEC

3.8.1 System Description

For our case study of a WEC we consider a cylinder with radius and draught equal to 5 m floating in deep water. For simplicity, we will only consider the heave motion of the WEC; however, most of the following considerations apply to systems with multiple degrees of freedom. To assess the effect of the time-domain method on the power performance, we will consider two PTO systems:

- Linear PTO
- Hydraulic PTO

3.8.1.1 Linear PTO

A model with a linear PTO is often produced to check the quality of the time-domain results comparing them with the ones given by the frequency domain. Eq. (3.1) can now be written as:

$$(M_{33}+A_{33}^{\infty})\ddot{x}_3(t)+\int_{-\infty}^{t}K_{33}(t-\tau)\dot{x}_3(\tau)d\tau + C_3x_3(t)+C_{\mathrm{PTO}}\dot{x}_3(t)=F_{e3}(t) \tag{3.81}$$

Eq. (3.81) can be represented using a system of two ODEs, where the buoy displacement and buoy velocity are the two states. The PTO force is in this case described by the product of a constant damping coefficient C_{PTO} (expressed in kg/s) and the buoy velocity (m/s). The instantaneous power absorbed by the buoy, therefore, is given by:

$$P(t)=C_{\mathrm{PTO}}\dot{x}_3(t)^2 \tag{3.82}$$

3.8.1.2 Hydraulic PTO

A frequently adopted PTO configuration for floating WECs is the one composed of a hydraulic circuit that converts the motion of the device into pressurized oil flow. There are several designs for this system and different modelling approaches might be used (Josset et al., 2007; Hals et al., 2007; Babarit et al., 2009; Ricci et, al., 2011), depending on the purpose of the model (whether

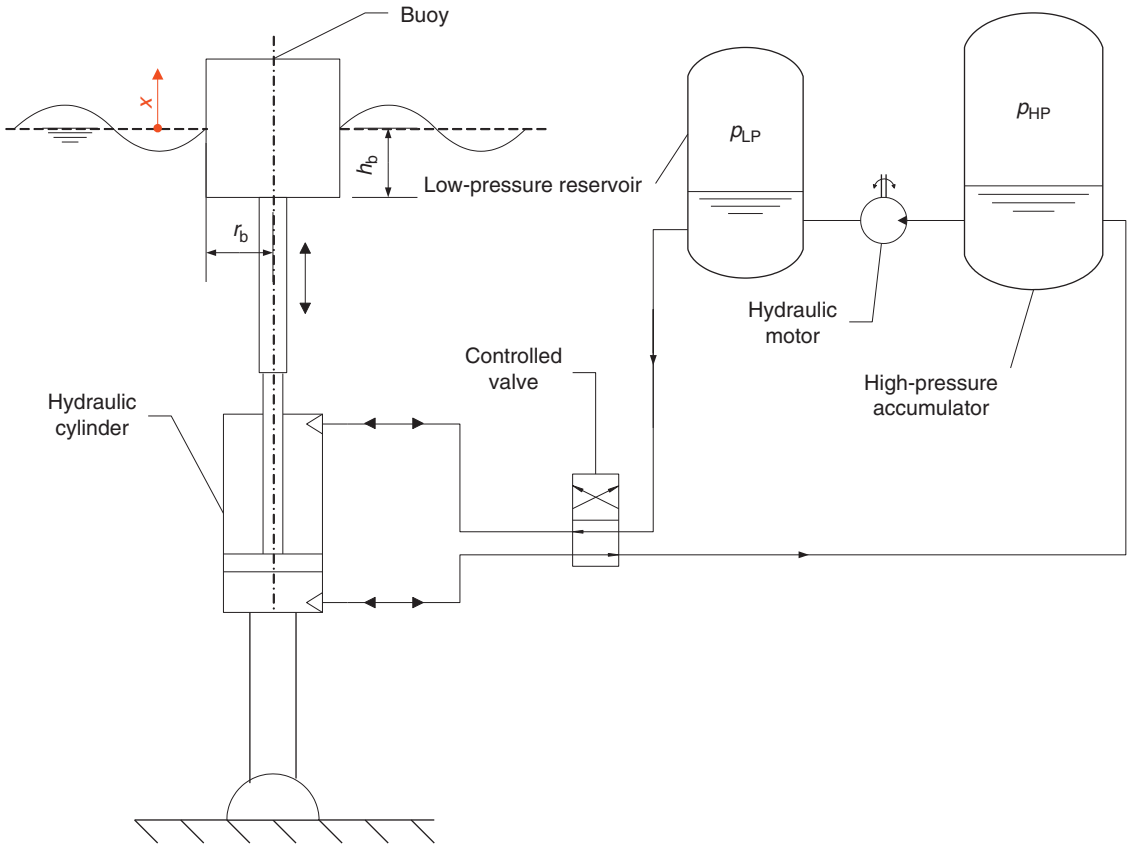

FIG. 3.9 Simplified representation of a wave point-absorber with hydraulic PTO.

to assess the feasibility of certain control strategies or to design its components).

Here we consider a simple PTO system that has been extensively studied by Falcão (2007), and applied by Candido and Justino (2011) for the case of a two-body system.

Fig. 3.9 shows the scheme considered for a preliminary validation of the methods. The circuit includes a hydraulic cylinder, a high-pressure (HP) gas accumulator, a low-pressure (LP) gas reservoir and a linear hydraulic motor. A controlled rectifying valve prevents the liquid from flowing out from the HP accumulator and flowing into the LP reservoir.

The dynamics can be described by a system of four ODEs

$$\begin{cases} \dot{y} = \dot{x}_3 \\ \ddot{y} = \dfrac{F_{e3}(t) - \int_{-\infty}^{t} K_{33}(t-\tau)\dot{x}_3(\tau)d\tau - \rho g S x_3 - S_{\text{pist}} \max\left((p_{\text{HP}} - p_{\text{LP}}), 0\right)}{M_{33} + A_{33}^{\infty}} \\ \dot{V}_{\text{HP}} = C_{\text{mot}} S_{\text{pist}}^2 \max\left((P_{\text{HP}} - P_{\text{LP}}), 0\right) - S_{\text{pist}}\dot{x}_3 \\ \dot{V}_{\text{LP}} = S_{\text{pist}}\dot{x}_3 - C_{\text{mot}} S_{\text{pist}}^2 \max\left((P_{\text{HP}} - P_{\text{LP}}), 0\right) \end{cases}. \tag{3.83}$$

where S_{pist} is the cross-sectional area of the piston inside the hydraulic cylinder, C_{mot} is a control parameter that regulates the flow to the motor as proposed in Falcão (2007) and p and V stand for pressure and volume with the subscript 'HP' and 'LP' identifying the related reservoir. Assuming the gas compression/expansion process inside the accumulators to be isentropic, p_{HP} and p_{LP} are given by

$$p_{\text{HP}} = \frac{p_{\text{HP},0} V_{\text{HP},0}^{1.4}}{V_{\text{HP}}^{1.4}} \; p_{\text{LP}} = \frac{p_{\text{LP},0} V_{\text{LP},0}^{1.4}}{V_{\text{LP}}^{1.4}} \tag{3.84}$$

where the subscript 0 stands for initial condition.

A condition must be included to avoid fluctuation around zero when the velocity changes sign. This is easy to impose if the velocity is set equal to zero whenever its sign changes over a time step and the hydrodynamic forces are not large enough to overcome the force due to the pressure difference between the two reservoirs. The instantaneous power absorbed by the buoy is expressed by the relation

$$P_b(t) = \max\left((p_{\text{HP}} - p_{\text{LP}}), 0\right) S_{\text{pist}}\dot{x}_3 \tag{3.85}$$

3.8.2 Design and Verification of Time-Domain Models

The first step in verification consists of comparing the dynamics computed by the time-domain model in regular waves with those predicted by the frequency-domain model. This allows the accuracy of the calculation of the hydrodynamic forces, and in particular the convolution integral, to be assessed. Since the solution in the time domain presents a transitory behaviour for the first few cycles, we will cut out the first 200 s from every realization. The average power is computed over the remaining time span, which must equal an integer number of wave periods, and compared to the values given by the frequency-domain analysis.

For the same three levels of PTO damping, Figs. 3.10 and 3.11 show the percentile error in the average power output given by Prony's method and direct numerical integration using a Crank–Nicolson solver, respectively. It can be seen that whilst Prony's methods have a very low error, the error in the direct numerical integration is much larger. As might be expected, direct integration methods are very sensitive to the step size so that a proper convergence study would be required if they were to be applied intensively in order to identify the maximum time step that guarantees a desired accuracy.

However, the error shown in Fig. 3.11 also appears to be very sensitive to the wave period. If we notice that the resonance period of the floating cylinder is actually equal to 5.8 s, we might associate this trend with inaccuracies in the computation of the convolution, whose contribution to the dynamics is most important close to resonance (when the motion amplitudes of the device are larger). This is somewhat supported by the fact that the error of the power

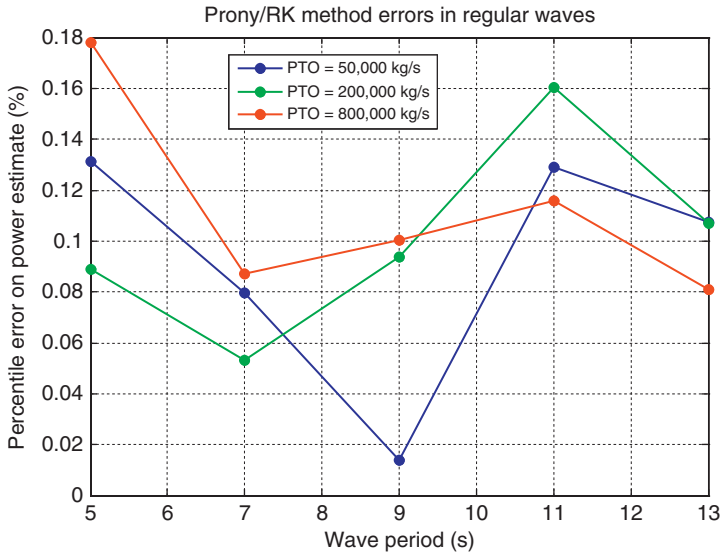

FIG. 3.10 Percentile error on the power estimate in regular waves of a floating cylinder with $r_b = h_b = 5$ m with linear PTO, computed using Prony method and variable step fourth/fifth-order Runge–Kutta.

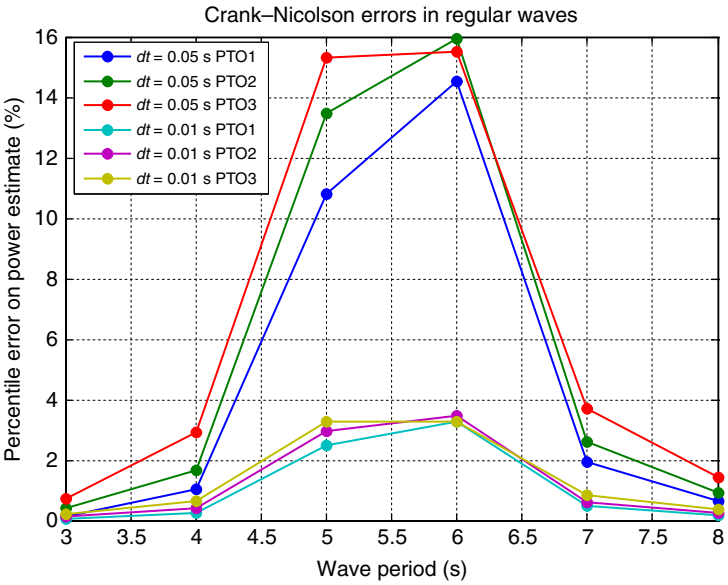

FIG. 3.11 Percentile error on the power estimate in regular waves of a floating cylinder with $r_b = h_b = 5$ m with linear PTO, computed using direct integration of the RIRF and Crank–Nicolson.

TABLE 3.1 Initial Values of the Gas Accumulator Pressures and Volumes

	Pressure (bar)	Volume (m^3)
HP accumulator	70	**7**
LP accumulator	**1.85**	**1**

TABLE 3.2 Average Powers Produced by the System With $H_s=2$ m and $T_e=7$ s

	P_{bhyd} (kW)
Prony–RK	34.38
Realization–RK	34.37
Backward Euler	30.61
Crank–Nicolson	33.59

computed by Prony's method does not show this behaviour and it appears to be independent of the wave period.

The next step is to compare the system responses for the hydraulic PTO in irregular waves, in this case a target Bretschneider wave spectrum characterized by $H_s=2$ m and $T_e=7$ s. Four different methods are considered.

- Prony's method and fourth/fifth-order Dormand–Prince Runge–Kutta solver
- Realization method and fourth/fifth-order Dormand–Prince Runge–Kutta solver
- Direct numerical integration and Backward Euler solver with a time step of 0.05 s
- Direct numerical integration and Crank–Nicolson solver with a time step of 0.05 s

In all cases the model uses a motor coefficient $C_{mot}=6\times10^{-7}$ s/kg and a piston with surface area equal to $S_{pist}=3.14\times10^{-2}$ m^2 (a radius of 10 cm). Table 3.1 summarizes the parameters set for the accumulators.

Fig. 3.12 compares the buoy motion for the four different methods. Because the hydraulic PTO is highly nonlinear, it can be seen that the buoy will tend to remain stationary from time to time, due to the sum of the hydrodynamic

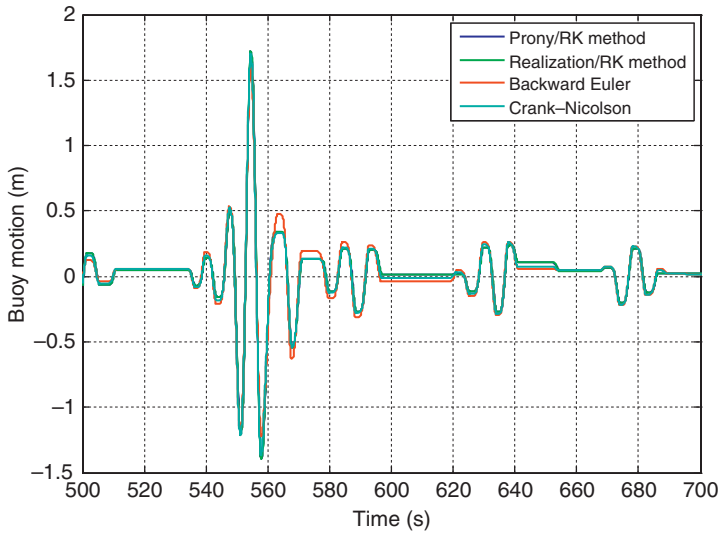

FIG. 3.12 Sample of motion response of a hydraulic PTO system with condition as set in Table 3.1 and with $H_s=2$ m and $T_e=7$ s.

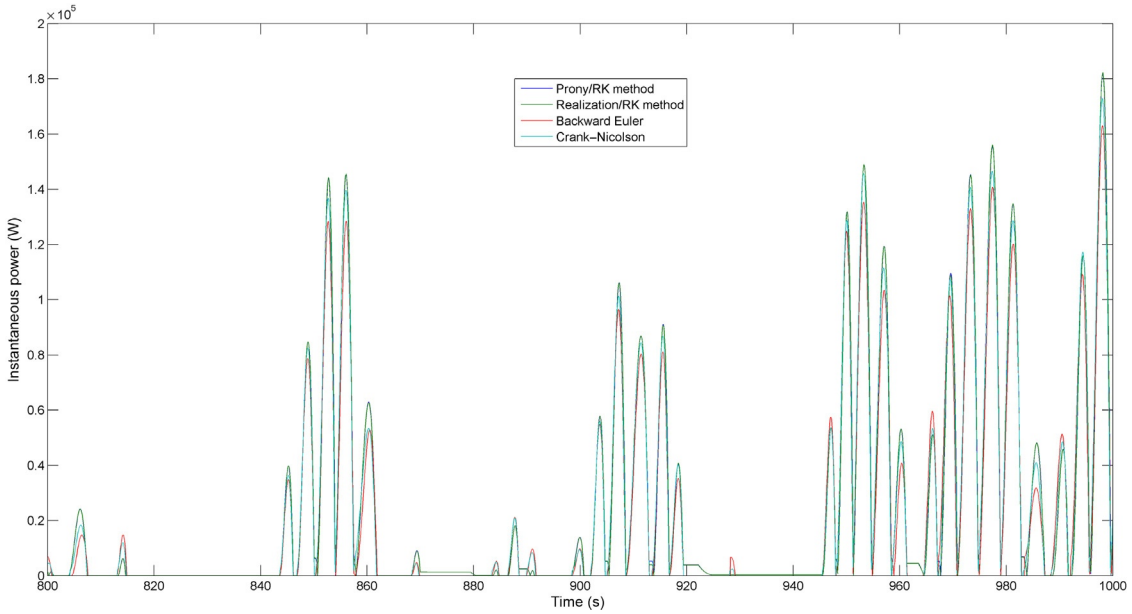

FIG. 3.13 Sample of power to the buoy response of a hydraulic PTO system with condition as set in Table 3.1 and with $H_s = 2$ m and $T_e = 7$ s.

and hydrostatic forces being smaller than the PTO force. The comparison of the power capture for the four methods is shown in Fig. 3.12 while the average power captures are given in Table 3.2. It can be seen that although the motions appears to be a little different (especially for the Backward Euler solver) the difference in power capture is less than 10%. Whether this is significant depends on the required accuracy of the model.

With only this set of data it is impossible to determine what is the 'correct' response and power capture. Convergence testing, with smaller time steps and more refined representations of the convolution integral would be required to determine this. However, the results from the initial verification tests suggest that a time step of 0.05 s is too long for a fixed-step solver and a shorter time step would be more appropriate. Moreover, the almost identical results for the Prony and realization methods with a variable-step solver suggest that these are calculating the 'correct' response and power capture (Fig. 3.13).

3.9 THE INFLUENCE OF SIMULATION DURATION

For a given wave spectrum there are an infinite number of possible wave elevation time series that have the same spectral characteristics. It turns out that differences in the wave elevation time series, apart from affecting the time-varying quantities, also influence the time-averaged power. Another possible factor of biases on the averaged quantities is the numerical method used to solve the ODEs. If the methods are accurate, there should be no significant difference between the application of one or another. There are, however, methods that are more time-consuming than other ones and it is not clear how much the numerical

parameters for the solution affect the estimation of the power production.

The simulation duration (T_d) plays an important role in the estimation of the expected power capture $\bar{P}$ of the WEC in a given sea-state. Intuitively, one can expect that the longer the total simulation duration, the better the estimate of the expected power capture. This total simulation could be from a single long simulation or from a number of shorter simulations, with the expected power capture being equal to the average of the mean power captures from each simulation.

For a linear system excited by Gaussian random waves as defined in Section 3.3 the system response (namely the velocities and displacements) also constitutes a Gaussian process (Papoulis, 1991). Subsequently, it is possible to show that the precision of the expected power capture obtained from time-domain simulations increases with the square root of T_d. However, it is important to stress that the frequency response of the WEC as well as the spectral shape of the wave spectrum have a nonnegligible influence on the magnitude of the error. This point is beyond the scope of this book, but the reader might consult Saulnier et al. (2009) for a theoretical formulation of the influence of the spectral bandwidth on the standard deviation of the absorbed power.

The mean absorbed power $\bar{P}$ has been computed in the time domain for three simulation durations T_d (500, 1000, and 1500 s) for the linear model and six durations T_d (300, 600, 900, 1200, 1500, and 1800 s) for the hydraulic model. For each configuration, a sample of 300 simulations was run, of which the mean value and standard deviation were calculated. The mean absorbed power is calculated for linear and hydraulic PTO configuration averaging respectively Eq. (3.82) and Eq. (3.85) over the duration of the simulation, excluding a ramp time of 200 s in order to avoid the start-up transient.

Fig. 3.14 depicts the distribution of the mean absorbed power for the hydraulic PTO model for $T_d = 600$, 1200, and 1800 s using the Crank–Nicolson solver. It is important to notice how the duration of the simulation strongly influences the statistical dispersion of the average power. Although the expected value appears to be the same in all the three data sets, the variance of the samples is visibly decreasing as T_d increases as expected. Similar trends can be observed in the linear PTO case.

Fig. 3.15 shows a comparison, for a linear PTO configuration, between numerical time-domain results and theoretical ones (Ricci et al. 2008). For the mean power capture it can be seen that all the applied methods have overestimated the value given by a stochastic approach using a frequency-domain model. This is likely to be related to the number of frequency components considered in the simulations. In the case of the

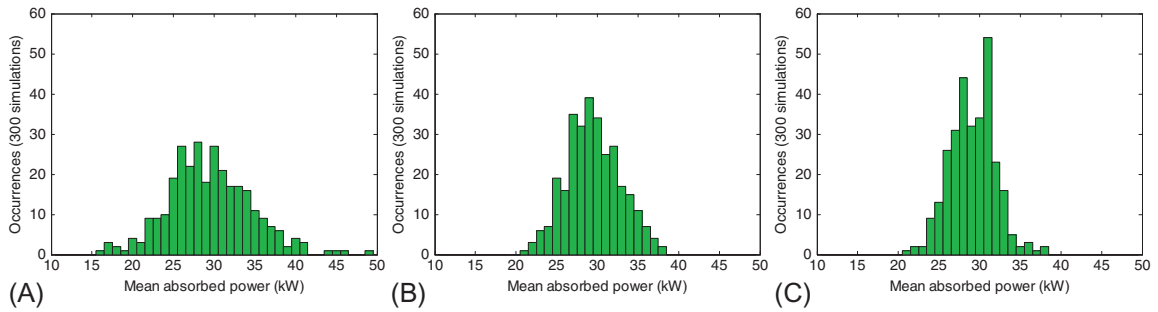

FIG. 3.14 Distribution of mean absorbed power for 300 simulations using Crank–Nicolson scheme (hydraulic PTO). (A) $T = 600$ s, (B) $T = 1200$ s, and (C) $T = 1800$ s.

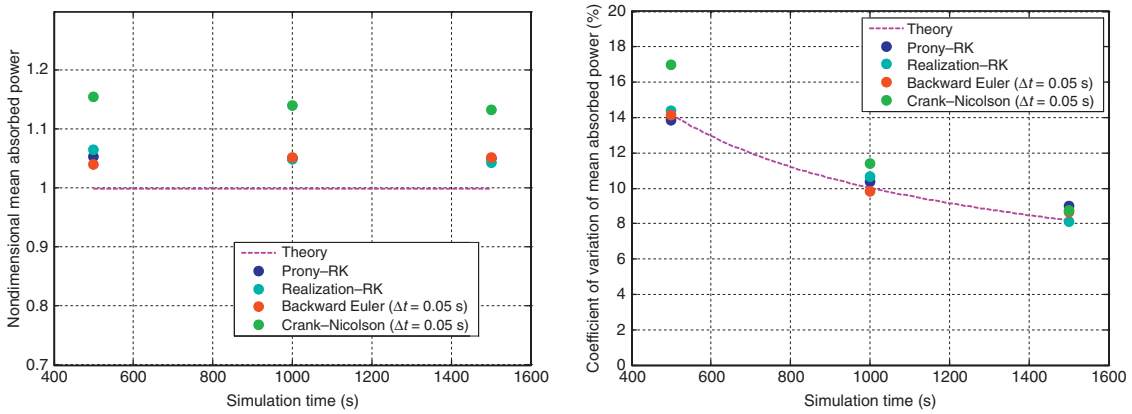

FIG. 3.15 Dimensionless absorbed power and coefficient of variation for the linear PTO model against duration of the simulation.

Crank–Nicolson method the error is significant at almost 15%.

Fig. 3.15 also shows a reasonable agreement between the estimated change in the coefficient of variation with simulation duration and the theory, although the Crank–Nicolson results seem to have more spread.

For the hydraulic PTO case, the correct power capture is unknown and, therefore, the mean power from all the methods for each duration is used for nondimensionalization in Fig. 3.16. In this case the results using the backward Euler method are significantly biased compared to the other methods. However, Prony and realization methods have similar results since the only difference between the two schemes is the representation of the system and the ODE solver. Fig. 3.16 also illustrates the trend of the relative standard deviation of the average power in function of the simulation duration. The results confirm that the standard deviation decreases with the inverse of the square root of the simulation duration (LS fitted curve).

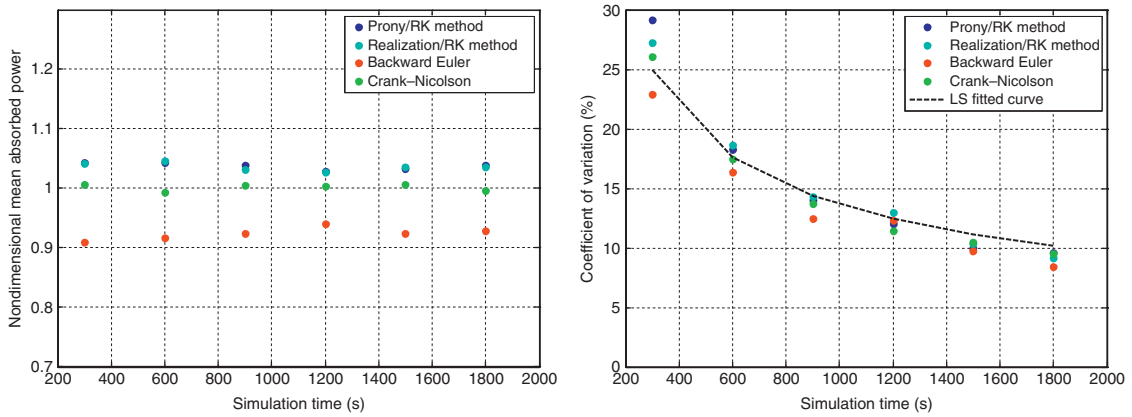

FIG. 3.16 Dimensionless absorbed power for the hydraulic PTO model against duration of the simulation.

3.10 LIMITATIONS

This chapter has given a glimpse of the capabilities of time-domain models for the numerical modelling of WECs. The main advantage of time-domain models is their applicability to any kind of system. In practice, virtually any type of WEC can be modelled by applying the methods described in this chapter, provided that the dynamics of the whole system can be modelled by a system of ODEs. However, there still are some limitations of this modelling technique.

First, the flexibility of the Cummins approach is limited by the fact that all forces need to be introduced as functions of the states of the system (eg, the buoy velocity) or the wave properties. Thus, extreme situations, where wave-breaking, slamming and other complex fluid phenomena may occur, cannot be modelled directly and require prior development of empirical formulae to relate these events to the system dynamic parameters.

It might seem obvious, but it is important to emphasize that the time-domain methods presented in this chapter require some idealization of the hydrodynamics so that they can be represented using a state-space model. The development of accurate and computationally efficient time-domain models for WECs does not overcome the underlying limitations of the Cummins formulation and the requirement to continuously validate the codes against model tests. In fact, in any exercise of calibrating numerical models against experiments, there is invariably a phase where empirically determined coefficients and/or formulations need to be introduced. Even though some standardization of time-domain codes is expected in the future, it is the author's opinion that none of these codes will ever be a substitute for engineering judgment and eliminate the requirement for conceptual development prior to any time-domain analysis.

Another important limitation of time-domain methods is their requirement for significant computational resources, at least in comparison to frequency-domain models. The models presented in this chapter were sufficiently simple to ensure convergence to a solution within few tens of seconds, even in the worst cases. This is unlikely to hold when modelling systems with multiple WECs and several degrees of freedom. Furthermore, the need for a large number of simulations to derive statistically significant quantities has the effect of making these models even more time-consuming.

This problem is somewhat amplified when complex control strategies are applied and the occurrence of abrupt changes in the system dynamics can slower considerably the solution in the time domain. In those cases, the user should choose the time-domain solver carefully since there are specific solvers suitable to deal with 'stiff' systems that can be applied. Even if the computational time is kept to a few minutes per simulation, the application of time-domain models might still be inappropriate in some cases, particularly when optimization of several design parameters (Chapter 12) is sought or where the mean annual average power capture needs to be determined using a large number of sea-states (Chapter 13).

Additionally, time-domain models have themselves their own sources of inaccuracies associated with the number of frequency components, truncation and discretization in the numerical integration and application of the correct solver. Thus, a time-domain model should not be considered more accurate than a frequency-domain model per se. On the contrary, its performance and suitability should be evaluated according to the context and the requirements of the analysis.

Since time-domain methods are clearly only applicable to a finite duration, if they model the response of random stochastic processes like irregular waves, their output is subject to large

variability dependent on the input parameters and the spectral model used. This is not only due to the random nature of ocean waves but is also heavily influenced by the parameters used for the numerical solution (number of frequency components and duration of the simulation). When used for the definition of design parameters, this variability leads to the requirements of carrying out several simulations to derive statistical estimates that are sufficiently representative of the expected design values. As mentioned earlier, this increases the required computational time and makes it more complicated to postprocess the results from time-domain simulations. Furthermore, the accuracy of the estimators derived from these simulations is difficult to ascertain unless a large number of simulations are carried out.

This chapter has introduced some relations that provide guidance in estimating the power that a WEC absorbs in a specified sea-state. However, these formulae do not apply to the estimator of other quantities. For instance, the duration of the simulations has an important effect on the extreme value estimation from time-domain simulations in irregular waves and the literature on the determination of their confidence range is scarce. Thus, when time-domain models are applied for the WEC performance assessment or the definition of design parameters (eg, structural loads, mooring line tensions), it is recommended to carry out the analysis on a large number of cases per each sea-state. In any case, statistical postprocessing of the results obtained is absolutely required and the analyst has to accept the occurrence of uncertainties in the estimation of the design parameters.

3.11 SUMMARY

- The Cummins equation and a state-space representation provide the underlying structure for these time-domain models
- The core hydrodynamic coefficients and forces are typically derived from linear potential flow models
- The capability to include additional nonlinear hydrodynamic and external forces makes this time-domain modelling technique extremely powerful
- The RIRF used in the convolution integral can be derived from the frequency-dependent radiation damping coefficient
- The radiation convolution integral in the Cummins equation can be replaced with a number of additional states using Prony, time-domain or frequency-domain identification techniques
- If care is not taken in the formulation of a time-domain model, significant errors can occur in the modelled response
- The accuracy of the estimated expected power capture and WEC response depends on the model formulation, the ODE solver and the simulation duration
- The uncertainty of the estimated expected power capture and WEC response decreases with the square root of the simulation duration
- Time-domain models are computationally demanding in comparison to frequency-domain models and may be unsuitable where a large number of simulations are required

References

Al-Saggaf, U.M., Franklin, G.F., 1987. An error-bound for a discrete reduced order model of a linear multivariable system. IEEE Trans. Autom. Control AC-32, 815–819.

ANSYS AQWA, 2010. ANSYS AQWA brochure. http://www.ansys.com/Products/Other+Products/ANSYS+AQWA (accessed 01.02.12).

Armesto, J.A., Guanche, R., del Jesus, F., Iturrioz, A., Losada, I.J., 2015. Comparative analysis of the methods to compute the radiation term in Cummins' equation. J. Ocean. Eng. Mar. Energy 1, 377–393.

Babarit, A., Clément, A.H., 2006. Optimal latching control of a wave energy device in regular and irregular waves. Appl. Ocean Res. 28, 77–91.

Babarit, A., Duclos, G., Clément, A.H., 2005. Comparison of latching control strategies for a heaving wave energy device in random sea. Appl. Ocean Res. 26, 227–238.
Babarit, A., Guglielmi, M., Clément, A.H., 2009. Declutching control of a wave energy converter. Ocean Eng. 36 (12–13), 1015–1024.
Bazaraa, M.S., Sherali, H.D., Shetty, C.M., 2006. Nonlinear Programming. John Wiley and Sons, New York, NY.
Candido, J.J., Justino, P.A.P., 2011. Modelling, control and Pontryagin Maximum Principle for a two-body wave energy device. Renew. Energy 36 (5), 1545–1557.
Chakrabarti, S., 2005. Handbook of Offshore Engineering. Elsevier, London. ISBN 978-0-08-044381-2.
Clément, A.H., 1995. Identification de la fonction de green de l'hydrodynamique transitoire par des modèles continus. In: Proc. 5èmes Journées de l'Hydrodyn, pp. 319–332.
Clément, A.H., 1999. Using differential properties of the green function in seakeeping computational codes. In: Proceedings of the Seventh International Conference on Numerical Ship Hydrodynamics, Paris, France, pp. 1–15.
Conte, S.D., De Boor, C., 1980. Elementary Numerical Analysis: An Algorithmic Approach. McGraw-Hill Ed., New York.
Cummins, W.E., 1962. The impulse response function and ship motions. Schiffstechnik 9 (1661), 101–109.
Damaren, C.J., 2000. Time-domain floating body dynamics by rational approximation of the radiation impedance and diffraction mapping. Ocean Eng. 27, 687–705.
de Prony, B.R., 1795. Essai expérimental et analytique sur les lois de dilatabilité des fluides élastiques et sur celles de la force expansive de la vapeur de la eau et de la vapeur de l'alcool à différentes températures. École polytechnique 1 (2), 24–76.
Duclos, G., Clément, A.H., Chatry, G., 2001. Absorption of outgoing waves in a numerical wave tank using a self-adaptive boundary condition. Int. J. Offshore Polar Eng. 11 (3), 168–175.
Falcão, A.F.d.O., 2007. Modelling and control of oscillating-body wave energy converters with hydraulic power take-off and gas accumulator. Ocean Eng. 34, 2021–2032.
Falnes, J., 1995. On non-causal impulse response functions related to propagating water waves. Appl. Ocean Res. 17, 379–389.
Falnes, J., 2002. Ocean Waves and Oscillating Systems: Linear Interactions Including Wave-Energy Extraction. Cambridge University Press, Cambridge.
Faltinsen, O., 1993. Sea Loads on Ships and Offshore Structures. Cambridge University Press, Cambridge.
Fusco, F., Ringwood, J., 2012. A study on the prediction requirements in real-time control of wave energy converters. IEEE Trans. Sust. Energ. 3 (1), 176–184.
Gilloteaux, J., Ducrozet, G., Babarit, A., Clément, A.H., 2007. Non-linear model to simulate large amplitude motions: application to wave energy converters. In: Proceedings of the 22nd IWWWFB, Plitvice, Croatia.
Greenhow, M., 1986. High- and low-frequency asymptotic consequences of the Kramers–Krönig relations. J. Eng. Math. 20, 293–306.
Hals, J., Taghipour, R., Moan, T., 2007. Dynamics of a force-compensated two-body wave energy converter in heave with hydraulic power take-off subject to phase control. In: Proceedings of the Seventh European Wave and Tidal Energy Conference, Porto, Portugal.
Ho, B., Kalman, R., 1966. Effective reconstruction of linear state-variable models from input/output functions. Regelungstechnik 14, 417–441.
Hoskin, R.E., Nichols, N.K., 1987. Optimal strategies for phase control of wave energy devices. In: McCormick, M.E., Kim, Y.C. (Eds.), Utilization of Ocean Waves: Wave to Energy Conversion. American Society of Civil Engineers, New York, NY, pp. 184–199.
Jefferys, E.R., 1980. Device characterization. In: Count, B.M. (Ed.), Power From Sea Waves. Academic Press, New York, NY, pp. 413–438.
Jefferys, E.R., 1984. Simulation of wave power devices. Appl. Ocean Res. 6, 31–39.
Josset, C., Babarit, A., Clément, A.H., 2007. A wave-to-wire model of the SEAREV wave energy converter. Proc. Inst. Mech. Eng. M J. Eng. Marit. Environ. 221 (2), 81–93.
Kashiwagi, M., 2004. Transient responses of a VLFS during landing and take-off of an airplane. J. Mar. Sci. Technol. 9 (1), 14–23.
King, B.K., Beck, R.F., 1987. Time-domain analysis of wave exciting forces. In: IWWWFB02—International Workshop on Water Waves and Floating Bodies, Bristol, UK, pp. 65–68. Host: D.V. Evans, University of Bristol.
Korsmeyer, F.T., 1991. The time-domain diffraction problem. In: IWWWFB06—International Workshop on Water Waves and Floating Bodies, Woods Hole, MA, USA, pp. 121–125. Host: J.N. Newman, MIT.
Korsmeyer, F.T., Bingham, H.B., Newman, J.N., 1999. TiMIT—A Panel Method for Transient Wave–Body Interactions. Research Laboratory of Electronics, MIT, Cambridge, MA.
Kotik, J., Mangulis, V., 1962. On the Kramers–Kronig relations for ship motions. Int. Shipbuild. Prog. 9, 361–368.
Kristiansen, E., Egeland, O., 2003. Frequency-dependent added mass in models for controller design for wave motion damping. In: Proceedings of Sixth Conference on Manoeuvring and Control of Marine Craft, Girona, Spain.
Kristiansen, E., Hjulstad, Å., Egeland, O., 2005. State-space representation of radiation forces in time-domain vessel models. Ocean Eng. 32, 2195–2216.
Kung, S., 1978. A new identification and model reduction algorithm via singular value decompositions. In: Proceedings of the 12th Asilomar Conference on Circuits, Systems and Computers, pp. 705–714.
Kurniawan, A., Hals, J., Moan, T., 2011. Assessment of time-domain models of wave energy conversion systems.

In: Proceedings of the Ninth European Wave and Tidal Energy Conference, Southampton, UK.
McCabe, A., Bradshaw, A., Widden, M., 2005. A time-domain model of a floating body using transforms. In: Proceedings of Sixth EWTEC, Glasgow, UK.
McCabe, A.P., Aggidis, G.A., Stallard, T.J., 2006. A time-varying parameter model of a body oscillating in pitch. Appl. Ocean Res. 28 (6), 359–370.
Ogilvie, T.F., 1964. Recent progress toward the understanding and prediction of ship motions. In: Proceedings of the Fifth Symposium on Naval Hydrodynamics, Bergen, Norway, pp. 3–79.
Papoulis, A., 1991. Probability, Random Variables, and Stochastic Processes. McGraw-Hill Series in Electrical Engineering. McGraw-Hill, New York.
Perez, T., Fossen, T., 2008a. Time-domain versus frequency-domain identification of parametric radiation force models for marine structures at zero speed. Model. Identif. Control. 29 (1), 1–29.
Perez, T., Fossen, T.I., 2008b. A derivation of high-frequency asymptotic values of 3D added mass and damping based on properties of the Cummins' equation. J. Marit. Res. 5 (1), 65–78.
Perez, T., Fossen, T.I., 2009. A Matlab toolbox for parametric identification of radiation-force models of ships and offshore structures. Model. Identif. Control. 30 (1), 1–15.
Perez, T., Fossen, T.I., 2011. Practical aspects of frequency-domain identification of dynamic models of marine structures from hydrodynamic data. Ocean Eng. 38, 426–435.
Pinkster, J.A., 1980. Low Frequency Second Order Wave Exciting Forces on Floating Structures. (Ph.D. thesis). Delft University of Technology.
Ricci, P., Saulnier, J.-B., Falcão, A.F.d.O., Teresa Pontes, M., 2008. Time-domain models and wave energy converters performance assessment. In: Proceedings of the 27th Offshore Mechanics and Arctic Engineering Conference, Estoril, Portugal.
Ricci, P., Lopez, J., Ruiz-Minguela, P., Villate, J.L., Salcedo, F., Falcão, A., 2011. Control strategies for a wave energy converter connected to a hydraulic power take-off. IET Renew. Power Gener. 5 (3), 234–244.
Riley, K.F., Hobson, M.P., Bence, S.J., 2006. Mathematical Methods for Physics and Engineering. Cambridge University Press, Cambridge.
Saulnier, J.-B., Ricci, P., Clément, A.H., Falcão, A.F.d.O., 2009. Mean power output estimation of WECs in simulated sea. In: Proceedings of the Eighth European Wave and Tidal Energy Conference, Uppsala, Sweden.
Sutulo, S., Guedes Soares, C., 2005. An implementation of the method of auxiliary state variables for solving seakeeping problems. Int. Shipbuild. Prog. 52 (4), 357–384.
Taghipour, R., Perez, T., Moan, T., 2008. Hybrid frequency-time domain models for dynamic response analysis of marine structures. Ocean Eng. 35 (7), 685–705.
Tedd, J., Frigaard, P., 2007. Short term wave forecasting using digital filters for improved control of wave energy converters. In: Proceedings of the 17th International Offshore and Polar Engineering Conference, Lisbon, Portugal.
WAMIT, 2004. WAMIT user manual. http://www.wamit.com (accessed Feb. 2012).
Wehausen, J.V., 1992. Causality and the radiation condition. J. Eng. Math. 26, 153–158.
Yu, Z., Falnes, J., 1996. State-space modelling of a vertical cylinder in heave. Appl. Ocean Res. 17, 265–275.